Enhancement of biotic degradation of terrestrial particulate organic matter in an estuarine salinity gradient: Interactive effects of organic matter pools and changes of bacterial communities.

Patricia Bonin, Anne-Hélène Prime, Mairie-Aimée Galeron, Sophie Guasco, Jean-Francois Rontani

Enhancement of biotic degradation of terrestrial particulate organic matter in estuarine salinity gradient: Interactive effects of organic matter pools and change of bacterial communities

Patricia Bonin*, Anne-Hélène Prime, Mairie-Aimée Galeron, Sophie Guasco and Jean-François Rontani

Aix Marseille Univ, Université de Toulon, CNRS, IRD, MIO UM 110, Marseille, France, 13288, Marseille, France.

**Correspondence to:patricia.bonin@mio.osupytheas.fr*

KEY WORDS: Estuaries; Terrestrial organic matter; Vascular plants; Biodegradation; Salinity; Potamoplankton.

ABSTRACT:

Suspended particulate matter **(**SPM) samples collected in the Rhône River during and after potamoplankton bloom were incubated *in vitro* at different salinities and the degradation of terrestrial vascular plants was monitored using specific lipid tracers (triterpenes, cuticular waxes and phenolic acids). Degradation was observed at a salinity close to that of seawater. Changes in salinity allow for the establishment of specific bacterial communities that seems to harbor bacteria possessing a capacity to degrade algal and vascular plant components more efficiently than these initially present within the river. The presence of potamoplankton (plankton of rivers) clearly enhanced remineralization of vascular plant material. The algal material resulting from the bloom event, which appeared to be intensively degraded during the incubations, could act as a co-substrate or induce the appearance of a bacterial community efficiently degrading terrestrial vascular plants. In SPM samples collected in the salinity gradient of the Rhône Estuary, bacterial degradation of vascular plant material increased with the proportion of algal sterols strongly suggesting the involvement of priming effect. Bacterial diversity analyses showed the dominance of Betaproteobacteria in freshwater and Alphaproteobacteria and Gammaproteobacteria in seawater. These results revealed the importance of potamoplankton and of the structure of bacterial communities during the degradation of terrestrial vascular plant material in estuaries.

INTRODUCTION

The riverine export of organic matter, whether dissolved or particulate is the main land-to-ocean contributor in coastal carbon fluxes. Early estimations ranged that contribution between 0.2 and 1 PgC yr^{-1} (Kempe 1979, Meybeck 1982), while more recent estimates limited that number to 0.45 PgC yr^{-1} (Cole et al. 2007) or 0.15 PgC yr^{-1} (Hedges et al. 1997). Given the current importance of exhaustive and precise carbon budgets and fluxes, it is crucial to look at the behavior of organic matter upon its arrival in coastal ecosystems.

The fate of terrestrial organic matter in the ocean is not fully understood (Handa 1977 ; Hedges et al. 1997) and the importance of this knowledge for global carbon-cycle understanding was evidenced long ago thanks to carbon isotope mass balance models (Berner, 1989). It has long been thought that the fraction of terrestrial vascular plant derived organic matter reaching estuarine areas was refractory to further degradation, mostly due to its intense degradation on land and in the rivers and its high lignin content (Bader 1956, De Leeuw & Baas 1993, Wakeham & Canuel 2006). However, it appears that only a small fraction of the organic matter found in coastal sediments is of terrestrial origin (Hedges et al. 1997), implying that either the estimations of current carbon reservoirs are incorrect, or, more likely, that organic matter undergoes an intense degradation upon reaching seawater (Hedges et al. 1997). Recent estimates of CO_2 efflux from streams and rivers confirmed that terrestrial organic carbon is not as recalcitrant as previously thought (Mayorga et al. 2005). It was recently estimated that over half of the Terrestrial Particulate Organic Matter (TPOM) is remineralized prior to burial (Kandasamy & Nagender Nath 2016).

Over the past decade, a number of studies evidenced that TPOM discharged by rivers was prone to remineralization in coastal areas in polar, temperate and tropical climate zones (Mayer et al. 2008, van Dongen et al. 2008, Vonk et al. 2010, Bourgeois et al. 2011, Rontani et

62 al. 2014). This efficient mineralization in the marine environment could be attributed to a more
63 efficient use of TPOM by marine bacterial assemblages than by their soil and river counterparts
64 (Garneau et al. 2009). The involvement of 'priming effects' (enhanced remineralization of
65 TPOM in the presence of fresh substrates from algal sources; (Steen et al. 2016)) constitutes
66 another possibility (Bianchi 2011, Bianchi et al. 2015, Ward et al. 2016). Indeed, coastal deltaic
67 regions, which are characterized by a high input of TPOM, a high primary production and the
68 presence of microbial communities highly adaptable to physicochemical changes, are generally
69 considered to have a high priming potential (Bianchi 2011). Unfortunately, the priming effect
70 phenomenon has been very poorly studied by the scientific communities working on marine
71 and continental aquatic ecosystems (Guenet et al. 2010) and studies showed contrasting results
72 (Bengtsson et al. 2018). The meta-analysis of results from the literature by (Bengtsson et al.
73 2018) revealed a weak and non-significant priming effects across fresh water and marine
74 ecosystems. The high photooxidation state of TPOM in some regions could also be at the origin
75 of the intense biodegradation of this material observed in seawater (Rontani et al. 2014). Indeed,
76 solar light-induced fragmentation can reduce structural barriers in higher plant debris and
77 expose new microniches to bacterial colonization (Vähätalo et al. 1998).
78 The present work is focused on the Rhône Estuary, where only 34% of the POM
79 discharged by the Rhône is deposited (Dufois et al. 2014). We intend to determine if the
80 presence of potamoplankton can enhance bacterial degradation of TPOM. Different hypothesis
81 are tested: i) an interactive effects of OM pools mixing and/or ii) a change in the microbial
82 community to a more adapted one with the increase of salinity. For this purpose, the degradation
83 of suspended particulate matter (SPM) collected in the Rhône River during and after the
84 potamoplankton bloom was studied *in vitro* at different salinities. Due to the overlapping
85 between $\delta^{13}C$ signatures of potamoplankton and terrestrial higher plants (Tolosa et al. 2013), it
86 was problematic to discern isotopically the sources of organic matter in the SPM samples, the

degradation of TPOM was thus monitored with several lipid tracers specific to terrestrial vascular plants (Table 1). At the same time, changes in the structure of bacterial communities were monitored both in the *in vitro* experiments and in SPM samples collected in the salinity gradient of the Rhône River mouth.

MATERIALS AND METHODS

Sampling

For the biodegradation experiments, fresh SPM samples were collected at the Arles station (43°40′44″N, 4°37′16″E, Fig. 1) on January 24 and March 30, 2017. At these sampling times, particulate organic matter contents were in the same range (31.6 and 36.7 g. Kg^{-1}, respectively). About 1000 l of Rhône River water were sampled at 1 m depth using a teflon-coated high-speed centrifuge (CEPA Z61), 42 and 56 g (wet weight) of SPM were obtained in January and March, respectively which were stored in an ice box until the return to the lab (1 h). After removal of SPM, the remaining freshwater was stored at 4°C. Collected SPM were used as bacterial inoculates and sources of TPOM upon arrival at the laboratory.

Sea water was sampled the 7 February 2017 at the station MESURHO (43° 19' 7"N, 4°51'58"E) near the Rhône River mouth (Fig. 1) in order to be used to adjust salinity for incubation and to gain the inoculum of marine bacteria. At sampling time, the salinity was 20 g kg^{-1} (Refractometer ATAGO ATC smile).

SPM samples were also collected in February 2012 along a transect following the salinity gradient in the Rhône flow in the framework of the national program MOOSE (Mediterranean Ocean Observing System for the Environment) (Fig. 1). The flow river was 980 m^3 s^{-1}. Five subsurface stations were sampled (between 0–3 m depth) with a Niskin bottle according to the salinity gradient: StA, StB, StC, StD and StE with 0, 15, 33, 39 and 40 g kg^{-1}, respectively (Fig.

1). The volume filtered (between 1 and 3 l) depended on SPM concentration at each station. The water was filtered on pre-combusted GF/F filters (Whatman). Filters were immediately frozen at –20 °C.

Biodegradation experiments

Two sets of biodegradation experiments were performed. The first one to mimic the effect of the variations of salinity on biodegradation of TPOM with SPM collected during the potamoplancton bloom in January. The second one to compare biodegradation of TPOM in bloom and post-bloom conditions. The experiments were performed in parallel; SPM sample collected on January 24 was stored less than 15 days after its collection. We cannot totally exclude a weak degradation of TPOM during the storage of this sample.

Experimental system were composed by 30 mg (equivalent dry weight) of fresh SPM collected at the Arles station in January or March 2017 and 150 ml of water adjusted at the chosen salinity (0, 10 or 20 g kg^{-1}) in 500 ml Erlenmeyer flasks. Fresh water (obtained from Rhône water after separation of SPM in January) and MESURHO sea water were used for incubations at 0 and 20 g kg^{-1}, respectively. Ten g kg^{-1} salinity was obtained by mixing sea water collected at the MESURHO station and Rhône fresh water. The dissolved organic carbon was in the same range in water from Rhône and MESURHO, it never exceeded 200 µM. The lipid content of the dissolved phase was considered as negligible relative to this of SPM.

Aerobic systems were incubated at a temperature close to the *in situ* temperature (15°C). To maintain aerobic conditions, flasks coated with cotton plugs were incubated in the dark on a reciprocal shaker (96 rpm, 5 cm amplitude). At each incubation time (0, 12, 24 and 38 days) three flasks (triplicates) were sampled, one for monitoring changes of bacterial biodiversity and two replicates for lipid analysis. All samples were filtered on pre-combusted GF/F filters (Whatman) and immediately frozen at –20 °C until analysis.

Chemical analysis

After defrosted, filters were placed in methanol (20 ml) with excess $NaBH_4$ (70 mg; 30 min at 20 °C). This operation was carried out in order to reduce hydroperoxides present in the samples (Galeron et al. 2015), which could induce autoxidative damages of lipids during the hot saponification step. After $NaBH_4$ reduction, 20 ml water and 2.8 g KOH were added and the mixture directly saponified by refluxing (75°C) for 2 h. After cooling, samples were acidified with HCl (pH 1) and extracted (3×) with dichloromethane (DCM). The combined DCM extracts were dried, evaporated to dryness and the total lipid extract (TLE) was dissolved in 300 µl of pyridine/N,O-bis(trimethylsilyl)trifluoroacetamide (BSTFA; Supelco; 2:1, v:v) and silylated for 1 h at 50 °C to convert OH-containing compounds to trimethylsilyl -ether or ester derivatives. After solvent removal under a stream of N_2, the derivatized residue was dissolved in 100 µl BSTFA (to avoid desilylation of FAs) and 600 µl of solvent (*n*-hexane).

GC–quadrupole time of flight mass spectrometry (GC–QTOF)

Accurate mass measurements were carried out in full scan mode with an Agilent 7890B/7200 GC–QTOF System (Agilent Technologies, Parc Technopolis - ZA Courtaboeuf, Les Ulis, France). A cross-linked 5% phenyl-methylpolysiloxane (Agilent; HP-5MS ultra inert) (30 m × 0.25 mm, 0.25 µm film thickness) column was used. Analysis was performed with an injector operating in pulsed splitless mode set at 270 °C and the oven temperature was programmed from 70 °C to 130 °C at 20 °C min^{-1} and then to 300 °C at 5 °C min^{-1}. The carrier gas (He) was maintained at 0.69×10^5 Pa until the end of the temperature program. Instrument temperature was 300 °C for the transfer line and 230 °C for the ion source. Accurate mass spectra were recorded across the range *m*/*z* 50–700 at 4 GHz. The instrument provided a typical resolution

ranging from 8009 to 12252 from *m/z* 68.9955 to 501.9706. Perfluorotributylamine (PFTBA) was utilized for daily MS calibration ($\Delta < 2$ ppm).

Standards

Quantification of lipids was carried out using GC-QTOF with external standards. Sitosterol, sitostanol, α-amyrin, β-amyrin, lupeol, vanillic, syringic and 4-hydroxycoumaric acids were obtained from Sigma-Aldrich. Cutin components (isomeric dihydroxyhexadecanoic acids) were quantified with a standard of 9-10-dihydroxyhexadecanoic acid obtained by oxidation of palmitoleic acid with OsO_4 (McCloskey & McClelland 1965).

Analysis of the bacterial communities associated to SPM

DNA extraction and PCR amplification

Genomic DNA was obtained from the filters using lysozyme-sodium dodecyl sulfate (SDS) followed by phenol-chloroform extraction and subsequent precipitation using ethanol. DNA concentration was determined spectrophotometrically following treatment with RNase. PCR amplification of bacterial 16SrRNA gene for DGGE analysis was performed using the GML5F – 907MR primer set for Bacterial community as previously described (Bonin et al. 2002, Goregues et al. 2005). For the ribosomal diversity analysis, the V4 region of the bacterial and archaeal 16S rRNA genes were amplified using a universal primer set, 515F-Y (5′-GTGYCAGCMGCCGCGGTAA-3′, (Parada et al. 2016) and 806RB (5′-GGACTACNVGGGTWTCTAAT-3′, (Apprill et al. 2015). PCR amplification was performed with 50 ng of target DNA and 0,5 µM (1 µL à 10 pmol/µL) of each primer. The reaction mixture contains 10 µL of GoTaq® PFU (Promega) in a final volume of 50 µl. PCR amplification is done in a minicycle (Biorad T100 Thermal Cycler) for 35 cycles. The matrix DNA is initially denatured for 3 minutes at 94°C. Each cycle includes a step of denaturing the double-stranded

186 DNA (45 seconds, 94°C), a step oligonucleotide hybridization (60 seconds, 50°C) and an
187 elongation step (90 seconds, 72°C). The amplification ends with a final elongation step at 72°C
188 for 10 minutes. Amplification products are detected by electrophoresis on agarose gel 1.5%
189 (Promega) followed by bromide staining ethidium (colored intercalant) ($1\mu g.ml^{-1}$).The 16S
190 rRNA gene amplicons were sequenced by the MiSeq Illumina (paired end 2* 250) platform Get
191 of Genotoul.

192

193 ***Diversity analysis***

194 The analysis of the biodiversity was performed by DGGE for the incubation samples whereas
195 prokaryotic diversity and community structure analysis was based on 16S rDNA- sequencing for the
196 salinity profile samples.
197 Denaturing Gradient Gel Electrophoresis (DGGE) was performed using a D-code Universal
198 Mutation Detection System (Bio-Rad Laboratories Inc.). Banding patterns across the gels were
199 normalized using a previously constructed ladder composed of seven different bands that was
200 loaded several times on each gel. Fingerprints observed on the gels were analyzed using
201 GelCompar II (Applied Maths, St-Martens-Latem, Be). After normalization, automatic band
202 detection was performed using a minimum profiling level of 5% relative to maximum. Band
203 comparison between different profiles was settled with a 2% position tolerance and a 1%
204 optimization to allow for tolerance of bands shifts within and among lanes. For DGGE patterns,
205 calculation of the pair-wise similarities of densitometric profiles was based on Pearson's
206 correlation coefficient (Michener & Sokal 1957) to construct dendrograms using the
207 Unweighted Pair-Group Method Analysis (GelCompar II software, Applied Maths, St-Martens-
208 Latem, Be).
209 The 16S amplicons were sequenced by the MiSeq Illumina (paired end 2 * 250) platform Get
210 of Genotoul. The paired-end raw reads were firstly overlapped and merged by platform GeT of

211 Genotoul. The analysis of the 16S-assembled data was relying on the use of QIIME 1.91
212 (Kuczynski et al. 2012). The removal of low quality bases and chimera sequences were
213 performed by QIIME 1.91 script and UCHIME (Edgar et al., 2011), respectively. The high-
214 quality sequences were next clustered into Operational Taxonomic Unit (OTU) using the
215 UCLUST algorithm and a threshold of 97% of sequence identity. The taxonomic assignment
216 of representative sequences of OTUs was performed using the green genes database (Edgar,
217 2010). The OTU table was filtered for low abundance OTUs (Bokulich et al., 2013). Finally,
218 sub-sampling normalization, alpha and beta diversity were characterized by Phyloseq, an open-
219 source software package project for R (www.r-project.org) (McMurdie and Holmes, 2013; R
220 Core Team, 2008).

221 **Statistical analyses**

222 The results were analyzed using the R® (GNU) software. Multivariate analyses (main
223 components (PCAs) and multiple factorials (MFAs)) were carried out in order to combine the
224 results of chemical and microbiological extractions. The influence of the different conditions
225 and incubation times were verified by mean (ANOVA) comparisons and Pearson or Spearman
226 correlations (normal data or not).

227

228 **RESULTS AND DISCUSSION**

229

230 **Lipid composition of SPM samples collected at the Arles station**

231 In SPM samples from the Rhône River (Fig. 1, StA), fatty acid (FA) profiles are generally
232 dominated by saturated FA and these of sterols by cholest-5-en-3β-ol (cholesterol) and 24-
233 ethylcholest-5-en-3β-ol (sitosterol) (Galeron et al. 2015) (See appendix). In contrast, the
234 sample collected in January appeared to contain high proportions of polyunsaturated FA ($C_{16:3}$,

$C_{16:4}$, $C_{18:4}$, $C_{20:3}$ and $C_{20:5}$), cholesta-5,24(25)-dien-3β-ol (desmosterol), 24-methylcholesta-5,22*E*-dien-3β-ol (brassicasterol) and 24-methylcholesta-5,24(28)-dien-3β-ol (24-methylenecholesterol) (Fig. S1A) (See appendix). This typical algal lipid composition confirmed the presence of the yearly potamoplanktonic bloom event, which was previously observed in the Rhône River (Galeron et al. 2015). The timing (ranging from January to March) and the intensity of this event seem to be strongly dependent on meteorological conditions (temperature, rainfall intensity and cloud cover thickness). On the basis of the high proportions of desmosterol and 24-methylenecholesterol detected, this bloom was attributed to freshwater diatoms. Indeed, 24-methylenecholesterol is the most common sterol in diatoms (Volkman 2003, Rampen et al. 2010) and desmosterol was proposed as a taxonomic marker for some species of diatoms, particularly for *Rhizosolenia*, where it is the dominant sterol (Barrett et al. 1995). This assumption is well supported by the drop of silica concentration observed at the same period (MOOSE data 2017, unpublished data).

In contrast, the SPM sample collected on March 7, 2017 exhibited a more classical lipid profile with very small proportions of PUFA, desmosterol and 24-methylenecholesterol attesting to the disappearance of the bloom (Fig. S1B).

The two samples (January and March) also contained: (i) isomeric dihydroxyhexadecanoic acids arising from the hydrolysis of cuticular waxes (von Wettstein-Knowles 1993, Otto et al. 2005) , (ii) a variety of pentacyclic triterpenoids with structures based on the ursene (α-amyrin and ursolic acid), oleanene (β-amyrin and oleanolic acid) or lupene (lupeol) hydrocarbon skeletons common in higher plant materials such as leaves, bark, roots and wood (Pancost & Boot 2004, Otto et al. 2005) and (iii) phenolic acids (vanillic, syringic, ferulic, 4-hydroxycoumaric acids) (Fig. S1). These last acids are generally considered as characteristic of lignin from non-woody vascular plant tissues (e.g., grass leaves, conifer needles) (Hedges & Mann 1979). They may also constitute ester-bound aromatic constituents of suberin

(Kolattukudy et al. 1981, Riederer et al. 1993, Kögel-Knabner 2002). It may be noted that ferulic acid and 4-hydroxycoumaric acid were also identified as components of ligno-cellulose complexes of grasses linking carbohydrates and lignin via ester bonds (Lam et al. 2001). Since the applied alkaline hydrolysis treatment cleaves esters, but not ethers, the phenolic acids detected are likely derived from ester-bound moieties of suberin and ligno-cellulose rather than from the ether-linked lignin macromolecule (Otto et al. 2005). 4-Hydroxycoumaric and ferulic acids (C) are only present in non-woody tissues of vascular plants, while syringic acid (S) is unique to angiosperms and vanillic acid (V) exists in all vascular plants (Table 1) (Sun et al., 2016). On the basis of the ratio C/V and S/V (Hedges and Mann, 1979) observed, TPOM carried by the Rhône River seems dominated by debris of angiosperm and grass leaves.

Isomeric dihydroxyhexadecanoic acids, α- and β-amyrins, lupeol, vanillic, syringic and 4-hydroxycoumaric acids were thus selected as tracers (Table 1) to monitor the degradation of TPOM during the different incubations. Sitosterol is also commonly associated with terrestrial higher plant inputs (Lütjohann 2004), but some microalgae (and notably diatoms) are also known to produce this sterol (Volkman 2003, Rampen et al. 2010). Due to the expected presence of high proportions of diatoms during the bloom event, a significant part of this sterol could not be traced back to higher plant material in SPM samples collected the 24th January, so we thus discarded the use of this widespread and ambiguous tracer during our *in vitro* studies of TPOM degradation.

Ex situ experiments to mimic variation of salinity and fresh algae input on bacterial degradation of TPOM

The bacterial degradation of TPOM was monitored with selected specific lipid tracers (Table 1) during the incubation of SPM collected in the Rhône River in January (during the bloom event) at different salinities (0, 10 and 20 g kg^{-1}) and at 15 °C. The decreasing concentrations

285 of 3β-hydroxy-urs-12-en-11-one and 3β-hydroxy-olean-12-en-11-one (specific tracers of α-
286 and β-amyrin autoxidation, respectively) ((Galeron et al. 2015, Galeron et al. 2016) observed
287 during these incubations allowed us to exclude the involvement of autoxidative artifacts. This
288 demonstrates that changes in the composition of these lipids observed during our incubations
289 were microbially mediated.

290 Cuticular wax components (isomeric dihydroxyhexadecanoic acids) and specific
291 triterpenes of vascular plants (α- and β-amyrins and lupeol) appeared to be degraded more
292 efficiently at the highest salinity (Table S1, Fig. 2A-C). It is interesting to note that this
293 degradation took place without accumulation of intermediate catabolites likely due to rapid
294 turnover. In the case of phenolic acids (vanillic, syringic and 4-hydroxycoumaric acids), a
295 decrease of their concentrations was observed at all salinities towards the end of the incubation
296 (Fig. 2D-F). However, in the case of the highest salinity an increase in the concentration could
297 be observed at the end of the incubation (Fig. 2D-F). This increase can be attributed to the
298 bacterial degradation of lignin, suberin or ligno-cellulose, well known to produce these acids
299 (Otto *et al.,* 2005). Indeed, in the literature there are a number of reports of bacteria
300 (*Streptomyces, Nocardia, Sphingomonas, Pseudomonas, Rhodococcus* …) that can break down
301 lignin structures and produce phenolic acids (for a review see (Bugg et al. 2011).

302 During the incubations, bacterial degradation also affected lipids of the algal
303 components of the bloom event. As in the case of TPOM, the extent of degradation of these
304 algal lipids increased with salinity ($C_{20:5}$ FA, desmosterol and phytol degradation percentages
305 ranging from 90, 70 and 40% at 0 g kg^{-1} to 95, 90 and 70% at 20 g kg^{-1}, respectively (data not
306 shown)).

307 A global analysis of the evolution of the structure of the bacterial community associated
308 to Rhône SPM by DGGE clearly shows the impact of salinity on bacterial communities.
309 Changes in salinity allow for the establishment of specific communities for each salinity,

310 dominated by different phylotypes (Fig. 3). The communities observed after incubation of
311 Rhône SPM at salinity 20 g kg^{-1} (T12, T24, T38) are close to those observed in situ at the same
312 salinity (greater than 50% similarity) (Fig. S2). This community seems to harbor bacteria
313 possessing higher capacities to degrade algal and vascular plant components than these initially
314 present within the river.
315

316 **Interactive effects of the presence of freshwater algae on the bacterial degradation of**
317 **TPOM**

318 Comparison of the bacterial TPOM biodegradation after incubation with the two kinds of SPM
319 (collected in January during the potamoplankton bloom or in March after this event) clearly
320 showed a faster degradation of cuticular wax components and triterpenes in the presence of
321 potamoplankton after incubation at the same salinity (20 g kg^{-1}) (Table S1, Fig. 4A-C).
322 Interestingly, the increase in phenolic acid concentration (attributed to lignin or suberin
323 degradation) observed at the end of the incubations with January SPM was not observed in the
324 case of incubations with March SPM (Table S2, Fig. 4D-F). The presence of freshwater
325 phytoplankton (dominated by diatoms) thus enhances TPOM remineralization. TPOM was
326 more intensively degraded with January SPM in the presence of high level of potamoplankton,
327 which could have a beneficial interactive effect on these processes or induce a change in
328 microbial communities.
329

330 **In situ behavior of TPOM in the salinity gradient of the Rhône River**
331

332 The stable carbon isotopic ($\delta^{13}C$) signatures of the main lipids (fatty acids and sterols) were
333 measured previously in the SPM samples collected along the salinity gradient of the Rhône

River (Galeron et al. 2018). Sitosterol (-27.1‰) was depleted in ^{13}C relative to 24-methylenecholesterol (–21.6‰) indicating a mainly terrestrial origin. We therefore used the percentage of sitostanol relative to the parent sitosterol for *in situ* TPOM bacterial degradation estimates. Indeed, stanols serve as useful indicators of bacterial degradation of Δ^5-sterols (Gagosian et al. 1982, Wakeham 1989, De Leeuw & Baas 1993). In the SPM samples collected in the Rhône Estuary, the percentage of sitostanol appeared to increase logarithmically from 0.4 to 15.4 % (Table S3) with the proportion of algal sterols (brassicasterol and 24-methylenecholesterol) relative to sitosterol (Fig. 5). The plateau observed at high proportions of algal material may be attributed to the well-known inhibition effect observed when co-substrates (algal sterols) and substrate (sitosterol) compete for the same enzymes (Dalton, 1982). Indeed, reduction of brassicasterol, 24-methylenecholesterol and sitosterol to the corresponding stanols involves the same enzymatic sequence. This enhancement of the biodegradation of sitosterol (arising mainly from terrestrial vascular plants in the Rhône River) (Galeron et al., 2015) with an increasing proportion of algal material (co-substrate) suggests that the presence of algal material favors TPOM degradation in the Rhône Estuary. Concerning the origin of the algal material present in these SPM samples, the relatively enriched $\delta^{13}C$ signature of 24-methylenecholesterol (a well-known diatom marker) (Volkman 2003, Rampen et al. 2010) allowed to exclude the presence of freshwater phytoplankton, which typically exhibits more depleted $\delta^{13}C$ values (–34‰ to –36‰) (Tolosa et al. 2013). The enhancement of the biotic degradation of TPOM in the salinity gradient of the Rhône River seems thus to result from the presence of marine diatoms.

The bacterial degradation of vascular plant material in the Rhône Estuary is well supported by: (i) the depleted carbon isotopic ($\delta^{13}C$) signatures (ranging from –30.9‰ to –27.8‰) of palmitoleic acid mainly arising from bacteria in the SPM samples investigated and (ii) the $\delta^{13}C$ signatures of the specifically bacterial vaccenic (-30‰) and branched

pentadecanoic (-29‰) acids previously measured by (Bourgeois et al. 2011) in sediments from the same deltaic region of the Rhône River. These different isotopic data confirm that bacteria present in the Rhône Estuary grew on ^{13}C depleted C3 terrestrial plant material and not ^{13}C enriched marine algae.

In situ biodiversity along the salinity gradient

The prokaryotic biodiversity was analyzed at different sampling sites along the salinity gradient in the Rhône River mouth. Five subsurface stations were sampled StA, StB, StC, StD and StE corresponding to the following salinities: 0, 15, 33, 38 and 39 g kg^{-1}. From the five libraries, 342123 sequences of 16S rRNA gene were analyzed (Table 2). Good's index showed that the sequencing depths were sufficient to cover 72.86 to 85.70 % of the microbial diversity (Table 2). The subdivision into operational taxonomic units (OTUs) sharing >97 % and after discarding low-quality read identity allowed the detection of the different OTUs (Table 2). A drastic decrease of species diversity was observed at the boundary between the two water masses (StA in the Rhône River and sea water, StB salinity 15g kg^{-1}) since both Shannon's diversity (H') and Simpson's diversity (D1) indexes (H' = 5.87, D1 = 0.93) were lower than in Rhône water (H' = 7.75 , D1 = 0.98) (Table 2). For higher salinities (StC, StD, StE) the diversity increases again, corresponding to a change in communities.

Rhône River communities was dominated by Proteobacteria (Alphaproteobacteria, Gammaproteobacteria and Betaproteobacteria). At intermediate salinity (15 g kg^{-1}), Betaproteobacteria strongly increased and new taxonomic classes were observed (Cytophagia, Flavobacteria). This community is also characterized by the presence of Actinobacteria. At salinities close to that of seawater Flavobacteria, Alphaproteobacteria, Gammaproteobacteria. and Thaumarchaeota dominated, while Betaproteobacteria were not detected (Figs 6 and 7).

384 Within the Proteobacteria classes, different families were observed within the salinity gradient.
385 Alphaproteobacteria are dominated by Rhodobacteraceae in freshwater and then
386 Pelagibacteraceae (at StB, 15 g kg^{-1}) and finally Rhodospirillaceae was detected as the salinity
387 increased (at StC, 33 g kg^{-1}). Among Gammaproteobacteria, Sinobacteraceae dominated in
388 freshwater, while Halomonadaceae and Alteromonadaceae were detected at salinities over 15
389 g kg^{-1}. Within Betaproteobacteria at StB, Rhodocyclaceae present in freshwater are substituted
390 by Comamonadaceae and Moraxellaceae, which then was progressively not detected with
391 increasing salinities (Fig. 6). Results indicated a significant change in the composition of the
392 microbial population all along the salinity gradient. In freshwater, the communities are
393 dominated by Betaproteobacteria; at StB, the communities are characterized by the presence of
394 Actinobacteria, whereas at the highest salinities Flavobacteria, Alphaproteobacteria and
395 Gammaproteobacteria were to be the most abundant. The dominance of Gamma and
396 Alphaproteobacteria in seawater and that of Betaproteobacteria in freshwater is in concordance
397 with the observations of (Newton et al. 2011) previously reported.

398 To unravel the relationships, the composition of the microbial community at the class
399 level taxonomy and the percentage of TPOM biodegradation, estimated from the ratio
400 sitostanol/sitosterol and the ratio (brassicasterol and 24-methylene cholesterol)/sitosterol
401 reflecting the amount of algal in the salinity gradient between, we performed a bi-plot MFA
402 (Fig. 7). The proportion of algal material strongly influences the biodegradation of sitosterol
403 (Fig. 7), which derives mainly from terrestrial plants in this area (Galeron et al. 2015). This
404 phenomenon seems to be of more relevance in seawater (at salinities of 39-40 g kg^{-1}) (Fig. 7).
405 The assimilative capacity of this recalcitrant organic material is therefore different according to
406 the communities present in the environment (Bianchi 2011). Interestingly, Crenarchaeota, more
407 abundant at intermediate salinities (33 g kg^{-1}) and well-known to degrade proteins and products
408 released by diatoms (co-substrate) more efficiently than bacteria (Kirchman et al. 2007) could

409 be also responsible for the enhancement of the degradation of TPOM. According to these
410 nutritional strategies, bacteria more efficient at degrading recalcitrant organic matter would be
411 located in the estuarine zone. Indeed, on the basis of the competitive exclusion principle,
412 generalist species (degrading recalcitrant compounds through priming and tolerant to changes)
413 should dominate diversified habitats (sea), while specialized species (in the degradation of the
414 TPOM) should live in a simplified environment (river) (Pimm et al. 1991, Kassen 2002).
415
416 **CONCLUSIONS**

417 In order to determine what phenomena are at the origin of the increase TPOM biodegradation
418 in seawater, SPM samples collected in the Rhône River during and after a bloom of
419 potamoplankton were incubated at different salinities (0, 15 and 20 g kg^{-1}). The degradation of
420 TPOM was monitored with specific lipid tracers (triterpenes, phenolic acids, cuticular wax
421 components). It appeared that TPOM was degraded more efficiently at the highest salinity and
422 in the presence of potamoplankton. The communities observed after incubation at the highest
423 salinity (20 g kg^{-1}), which are close to those observed *in situ* at the same salinity, degraded algal
424 and vascular plant components more efficiently than that present within the river. The enhanced
425 degradation of TPOM observed in the presence of potamoplankton (dominated by diatoms) is
426 likely due to the presence of an algal co-substrate or/and a more efficient bacterial community
427 during the bloom period. The bacterial consumption of TPOM observed in SPM samples
428 collected in 2012 in the salinity gradient of the Rhône River was attributed to: (i) the
429 involvement of priming effect, this process being likely induced by the presence of important
430 proportions of marine diatoms, or (ii) a more efficient use of TPOM by marine bacterial
431 assemblages than by their river counterparts. Indeed, the increase of salinity in the river mouth
432 results in an enrichment in Gammaproteobacteria, which seem to be more efficient degraders
433 of TPOM than Betaproteobacteria dominating the communities in the river.

Acknowledgements

This work was supported by the LEFE-CYBER (Les Enveloppes Fluides et l'Environnement) national program, as part of the MORTIMER (Matière ORganique Terrestre rejetée par les fleuves et les rIvières en MER) research program. This study is also a contribution to the Labex OT-Med (through ANR-11-LABX-0061) funded by the French Government "Investissements d'Avenir" program of the French National Research Agency (ANR) through the A*MIDEX project (ANR-11-IDEX-0001-02). Thanks are due to the FEDER OCEANOMED (N° 1166-39417) for the funding of the apparatus employed. Additional data were provided by "MOOSE" (Mediterranean Oceanic Observing System for the Environment) with the support of the "Agence de l'Eau Rhône-Méditerranée-Corse". We thank two anonymous referees for their useful and constructive comments.

REFERENCES

Apprill A, McNally S, Parsons R, Weber L (2015) Minor revision to V4 region SSU rRNA 806R gene primer greatly increases detection of SAR11 bacterioplankton. Aquatic Microbial Ecology 75:129-137

Bader R (1956) The lignin fraction of marine sediments. Deep-sea Research 4:15-22

Barrett SM, Volkman JK, Dunstan GA, LeRoi JM (1995) Sterols of 14 species of marine diatoms (Bacillariophyta). Journal of Phycology 31:360-369

Bengtsson MM, Attermeyer K, Catalán N (2018) Interactive effects on organic matter processing from soils to the ocean: are priming effects relevant in aquatic ecosystems? Hydrobiologia:1-17

Bianchi TS (2011) The role of terrestrially derived organic carbon in the coastal ocean: A changing paradigm and the priming effect. Proceedings of the National Academy of Sciences 108:19473-19481

Bianchi TS, Thornton DC, Yvon-Lewis SA, King GM, Eglinton TI, Shields MR, Ward ND, Curtis J (2015) Positive priming of terrestrially derived dissolved organic matter in a freshwater microcosm system. Geophysical Research Letters 42:5460-5467

Bonin PC, Michotey VD, Mouzdahir A, Rontani J-F (2002) Anaerobic biodegradation of squalene: using DGGE to monitor the isolation of denitrifying bacteria taken from enrichment cultures. FEMS microbiology ecology 42:37-49

Bourgeois S, Pruski A, Sun M-Y, Buscail R, Lantoine F, Kerhervé P, Vétion G, Rivière B, Charles F (2011) Distribution and lability of land-derived organic matter in the surface sediments of the Rhône prodelta and the adjacent shelf (Mediterranean Sea, France): a multi proxy study. Biogeosciences 8:3107

Bugg TD, Ahmad M, Hardiman EM, Rahmanpour R (2011) Pathways for degradation of lignin in bacteria and fungi. Natural product reports 28:1883-1896

Cole JJ, Prairie YT, Caraco NF, McDowell WH, Tranvik LJ, Striegl RG, Duarte CM, Kortelainen P, Downing JA, Middelburg JJ (2007) Plumbing the global carbon cycle: integrating inland waters into the terrestrial carbon budget. Ecosystems 10:172-185

De Leeuw J, Baas M (1993) The behaviour of esters in the presence of tetramethylammonium salts at elevated temperatures; flash pyrolysis or flash chemolysis? Journal of Analytical and Applied Pyrolysis 26:175-184

Dufois F, Verney R, Le Hir P, Dumas F, Charmasson S (2014) Impact of winter storms on sediment erosion in the Rhone River prodelta and fate of sediment in the Gulf of Lions (North Western Mediterranean Sea). Continental Shelf Research 72:57-72

Gagosian RB, Smith SO, Nigrelli GE (1982) Vertical transport of steroid alcohols and ketones measured in a sediment trap experiment in the equatorial Atlantic Ocean. Geochimica et cosmochimica acta 46:1163-1172

Galeron M-A, Amiraux R, Charriere B, Radakovitch O, Raimbault P, Garcia N, Lagadec V, Vaultier F, Rontani J-F (2015) Seasonal survey of the composition and degradation state of particulate organic matter in the Rhône River using lipid tracers. Biogeosciences Discussions:1431-1446

Galeron M-A, Radakovitch O, Charrière B, Vaultier F, Volkman JK, Bianchi TS, Ward ND, Medeiros PM, Sawakuchi HO, Tank S (2018) Lipoxygenase-induced autoxidative degradation of terrestrial particulate organic matter in estuaries: A widespread process enhanced at high and low latitude. Organic Geochemistry 115:78-92

Galeron M-A, Vaultier F, Rontani J-F (2016) Oxidation products of α-and β-amyrins: potential tracers of abiotic degradation of vascular-plant organic matter in aquatic environments. Environmental Chemistry 13:732-744
Garneau M-È, Vincent WF, Terrado R, Lovejoy C (2009) Importance of particle-associated bacterial heterotrophy in a coastal Arctic ecosystem. Journal of Marine Systems 75:185-197
Goregues C, Michotey V, Bonin P (2005) Molecular, biochemical, and physiological approaches forunderstanding the ecology of denitrification. Microbial ecology 49:198-208
Guenet B, Danger M, Abbadie L, Lacroix G (2010) Priming effect: bridging the gap between terrestrial and aquatic ecology. Ecology 91:2850-2861
Handa N (1977) Land sources of marine organic matter. Marine Chemistry 5:341-359
Hedges J, Keil R, Benner R (1997) What happens to terrestrial organic matter in the ocean? Organic geochemistry 27:195-212
Hedges JI, Mann DC (1979) The characterization of plant tissues by their lignin oxidation products. Geochimica et Cosmochimica Acta 43:1803-1807
Kandasamy S, Nagender Nath B (2016) Perspectives on the terrestrial organic matter transport and burial along the land-deep sea continuum: Caveats in our understanding of biogeochemical processes and future needs. Frontiers in Marine Science 3:259
Kassen R (2002) The experimental evolution of specialists, generalists, and the maintenance of diversity. Journal of evolutionary biology 15:173-190
Kempe S (1979) Carbon in the freshwater cycle. In: Bolin B, Degens ET, Kempe S, Ketner P (eds) The Global Carbon Cycle Book 13. John Wiley, New York
Kirchman DL, Elifantz H, Dittel AI, Malmstrom RR, Cottrell MT (2007) Standing stocks and activity of Archaea and Bacteria in the western Arctic Ocean. Limnology and Oceanography 52:495-507
Kögel-Knabner I (2002) The macromolecular organic composition of plant and microbial residues as inputs to soil organic matter. Soil Biology and Biochemistry 34:139-162
Kolattukudy P, Espelie K, Soliday C (1981) Hydrophobic layers attached to cell walls. Cutin, suberin and associated waxes. In: Plant Carbohydrates II. Springer
Kuczynski J, Stombaugh J, Walters WA, González A, Caporaso JG, Knight R (2012) Using QIIME to analyze 16S rRNA gene sequences from microbial communities. Current protocols in microbiology:1E. 5.1-1E. 5.20
Lam T, Kadoya K, Iiyama K (2001) Bonding of hydroxycinnamic acids to lignin: ferulic and p-coumaric acids are predominantly linked at the benzyl position of lignin, not the β-position, in grass cell walls. Phytochemistry 57:987-992
Lütjohann D (2004) Sterol autoxidation: from phytosterols to oxyphytosterols. The British journal of nutrition 91:3
Mayer LM, Schick LL, Allison MA (2008) Input of nutritionally rich organic matter from the Mississippi River to the Louisiana coastal zone. Estuaries and Coasts 31:1052-1062
Mayorga E, Aufdenkampe AK, Masiello CA, Krusche AV, Hedges JI, Quay PD, Richey JE, Brown TA (2005) Young organic matter as a source of carbon dioxide outgassing from Amazonian rivers. Nature 436:538
McCloskey JA, McClelland MJ (1965) Mass spectra of O-isopropylidene derivatives of unsaturated fatty esters. Journal of the American Chemical Society 87:5090-5093
Meybeck M (1982) Carbon, nitrogen, and phosphorus transport by world rivers. Am J Sci 282:401-450
Michener CD, Sokal RR (1957) A quantitative approach to a problem in classification. Evolution 11:130-162

Newton RJ, Jones SE, Eiler A, McMahon KD, Bertilsson S (2011) A guide to the natural history of freshwater lake bacteria. Microbiology and Molecular Biology Reviews 75:14-49
Otto A, Shunthirasingham C, Simpson MJ (2005) A comparison of plant and microbial biomarkers in grassland soils from the Prairie Ecozone of Canada. Organic Geochemistry 36:425-448
Pancost RD, Boot CS (2004) The palaeoclimatic utility of terrestrial biomarkers in marine sediments. Marine Chemistry 92:239-261
Parada AE, Needham DM, Fuhrman JA (2016) Every base matters: assessing small subunit rRNA primers for marine microbiomes with mock communities, time series and global field samples. Environmental microbiology 18:1403-1414
Pimm SL, Lawton JH, Cohen JE (1991) Food web patterns and their consequences. Nature 350:669
Rampen SW, Abbas BA, Schouten S, Sinninghe Damste JS (2010) A comprehensive study of sterols in marine diatoms (Bacillariophyta): implications for their use as tracers for diatom productivity. Limnology and oceanography 55:91-105
Riederer M, Matzke K, Ziegler F, Kögel-Knabner I (1993) Occurrence, distribution and fate of the lipid plant biopolymers cutin and suberin in temperate forest soils. Organic Geochemistry 20:1063-1076
Rontani J-F, Charrière B, Sempéré R, Doxaran D, Vaultier F, Vonk JE, Volkman JK (2014) Degradation of sterols and terrigenous organic matter in waters of the Mackenzie Shelf, Canadian Arctic. Organic Geochemistry 75:61-73
Steen IH, Dahle H, Stokke R, Roalkvam I, Daae F-L, Rapp HT, Pedersen RB, Thorseth IH (2016) Novel barite chimneys at the Loki's castle vent field shed light on key factors shaping microbial communities and functions in hydrothermal systems. Frontiers in microbiology 6:1510
Tolosa I, Fiorini S, Gasser B, Martín J, Miquel J (2013) Carbon sources in suspended particles and surface sediments from the Beaufort Sea revealed by molecular lipid biomarkers and compound-specific isotope analysis. Biogeosciences 10:2061-2087
Vähätalo A, Søndergaard M, Schlüter L, Markager S (1998) Impact of solar radiation on the decomposition of detrital leaves of eelgrass Zostera marina. Marine Ecology Progress Series:107-117
van Dongen BE, Zencak Z, Gustafsson Ö (2008) Differential transport and degradation of bulk organic carbon and specific terrestrial biomarkers in the surface waters of a sub-arctic brackish bay mixing zone. Marine Chemistry 112:203-214
Volkman JK (2003) Sterols in microorganisms. Applied microbiology and Biotechnology 60:495-506
von Wettstein-Knowles P (1993) Waxes, cutin and suberin. Lipid metabolism in plants:127-166
Vonk J, Sobczak W, Mann P, Bulygina E, Zimov S, Holmes R The Crucial Role of Particulate Matter in Fluvial Degradation of Thaw-Released Arctic Carbon. In. Proc AGU Fall Meeting Abstracts
Wakeham SG (1989) Reduction of stenols to stanols in particulate matter at oxic–anoxic boundaries in sea water. Nature 342:787
Wakeham SG, Canuel EA (2006) Degradation and preservation of organic matter in marine sediments. In: Marine organic matter: biomarkers, isotopes and DNA. Springer
Ward ND, Bianchi TS, Sawakuchi HO, Gagne-Maynard W, Cunha AC, Brito DC, Neu V, Matos Valerio A, Silva R, Krusche AV (2016) The reactivity of plant-derived organic matter and the potential importance of priming effects along the lower Amazon River. Journal of Geophysical Research: Biogeosciences 121:1522-1539

596 **Figure captions**

597

598 **Figure 1:** Summary map showing sampling locations.

599 **Figure 2:** Concentrations (ng mg^{-1}) of isomeric dihydroxyhexadecanoic acids (cuticular wax
600 components) (A), β-amyrin (B), lupeol (C), vanillic acid (D), syringic acid (E) and 4-
601 hydroxycoumaric acid (F) measured during incubations of Rhône SPM collected in January
602 after incubation at different salinities.

603 **Figure 3:** Multiple Factor Analysis (MFA), correlation biplot showing 16 samples (individual
604 factor map) and the correlation circle with the 8 most representative phylotypes (pink arrows,
605 migration distances observed in DGGE gels, Fig S2), geochemical tracers (phytol, waxes,
606 β–amyrin, α–amyrin, ursolic acid, blue arrow) and salinity (red arrows), The PCA accounts for
607 58.6 % of the total variation incubation conditions (Axis 1:35.77% and Axis 2:22.77 %).
608 Samples were identified as their incubation time (T0, T12, T24 or T38 incubation days)
609 followed by their salinity (0 g kg^{-1} (S0), 10 g kg^{-1} (S10) or 20 g kg^{-1} (S20)).

610 **Figure 4:** Concentrations (ng mg^{-1}) of isomeric dihydroxyhexadecanoic acids (cuticular wax
611 components) (A), β-amyrin (B), lupeol (C), vanillic acid (D), syringic acid (E) and 4-
612 hydroxycoumaric acid (F) measured during incubations of Rhône SPM collected in January and
613 March at the salinity of 20 g kg^{-1}.

614 **Figure 5:** Biodegradation percentage of TPOM (estimated with the ratio sitostanol / sitosterol)
615 in relation to the proportion of algal sterols (estimated with the ratio (brassicasterol + 24-
616 methylenecholesterol) / sitosterol) in SPM samples collected in 2012 in the Rhône River and
617 Mouth (salinity gradient).

618

Figure 6: Percentages of abundance of OTUs, classed at family level and ranked according to their class. Samples collected in 2012 at the Rhône (Arles) station (StA) and in the salinity gradient (StB, StC, StD and StE at 15, 33, 39 and 40 g kg^{-1}, respectively).

Figure 7: Multiple Factor Analysis (MFA), correlation biplot showing 5 samples (collected in the salinity gradient of the Rhône River plum in 2012) and the correlation circle with the 9 most representative class (pink arrows, see figure 6), Biodegradation rate (blue arrow), amount of co substrate (red arrow) and salinity (green arrows), The MFA accounts for 75.4 % of the total variation incubation conditions (Axis 1:49.99% and Axis 2:25.41%).

Figure S1: TOF mass chromatograms of the silylated total lipid extract of SPM collected in the Rhône River at the Arles station during (the 24/01/2017) (A) and after (the 30/03/2017) (B) the potamoplankton bloom event.

Figure S2: Dendrogram from DGGE analyses of the evolution of the bacterial community according to Jaccard's indexes and the classification algorithm hierarchy UPGMA (Unweighted Pair Group Method with Arithmetic mean) samples according to time incubation (0 (T0), 12 (T1), 24 (T2) or 38 (T3) days of incubation) and the water salinity (0 g kg^{-1} (S0), 10 g kg^{-1} (S10) or 20 g kg^{-1} (S20)).

APPENDIX

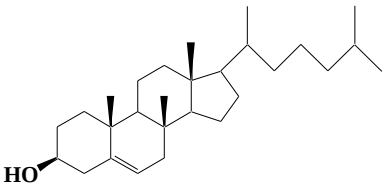

Cholesterol

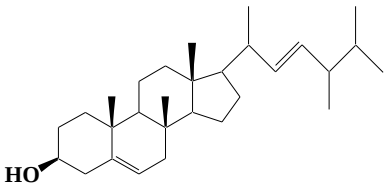

Brassicasterol

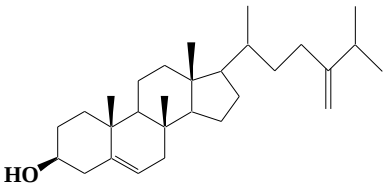

24-Methylenecholesterol

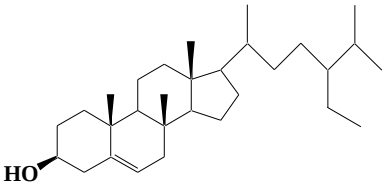

Sitosterol

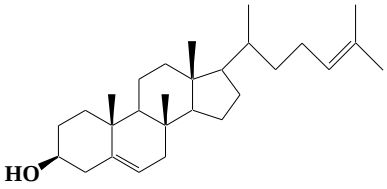

Desmosterol

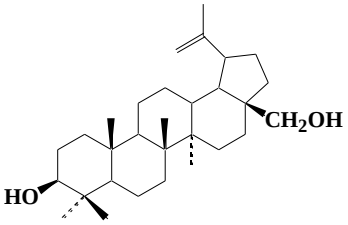

Betulin

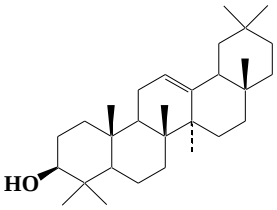

β-amyrin

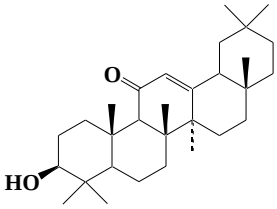

11-Oxo-β-amyrin

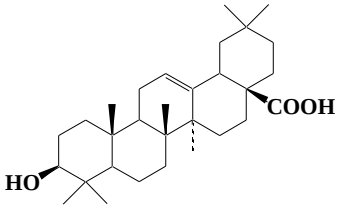

Oleanolic acid

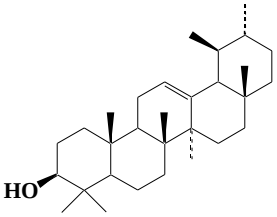

α-amyrin

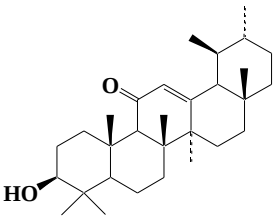

11-Oxo-α-amyrin

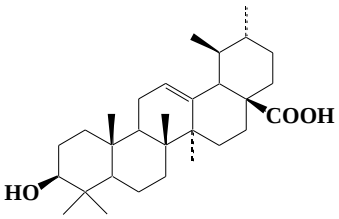

Ursolic acid

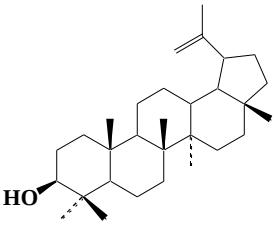

Lupeol

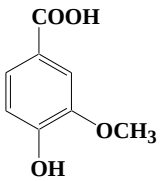

Vanillic acid

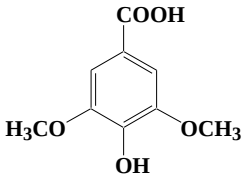

Syringic acid

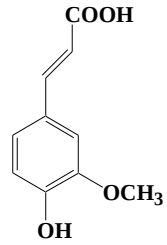

Ferulic acid

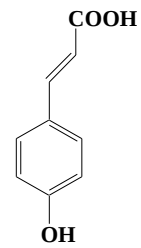

4-Hydroxy cinnamic acid

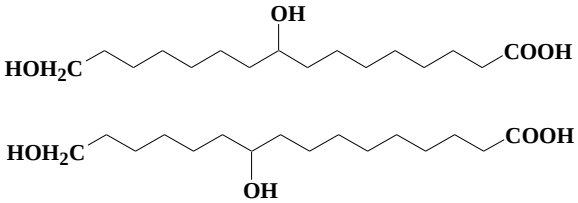

Isomeric dihydroxyhexadecanoic acids
(Cutin components)

638

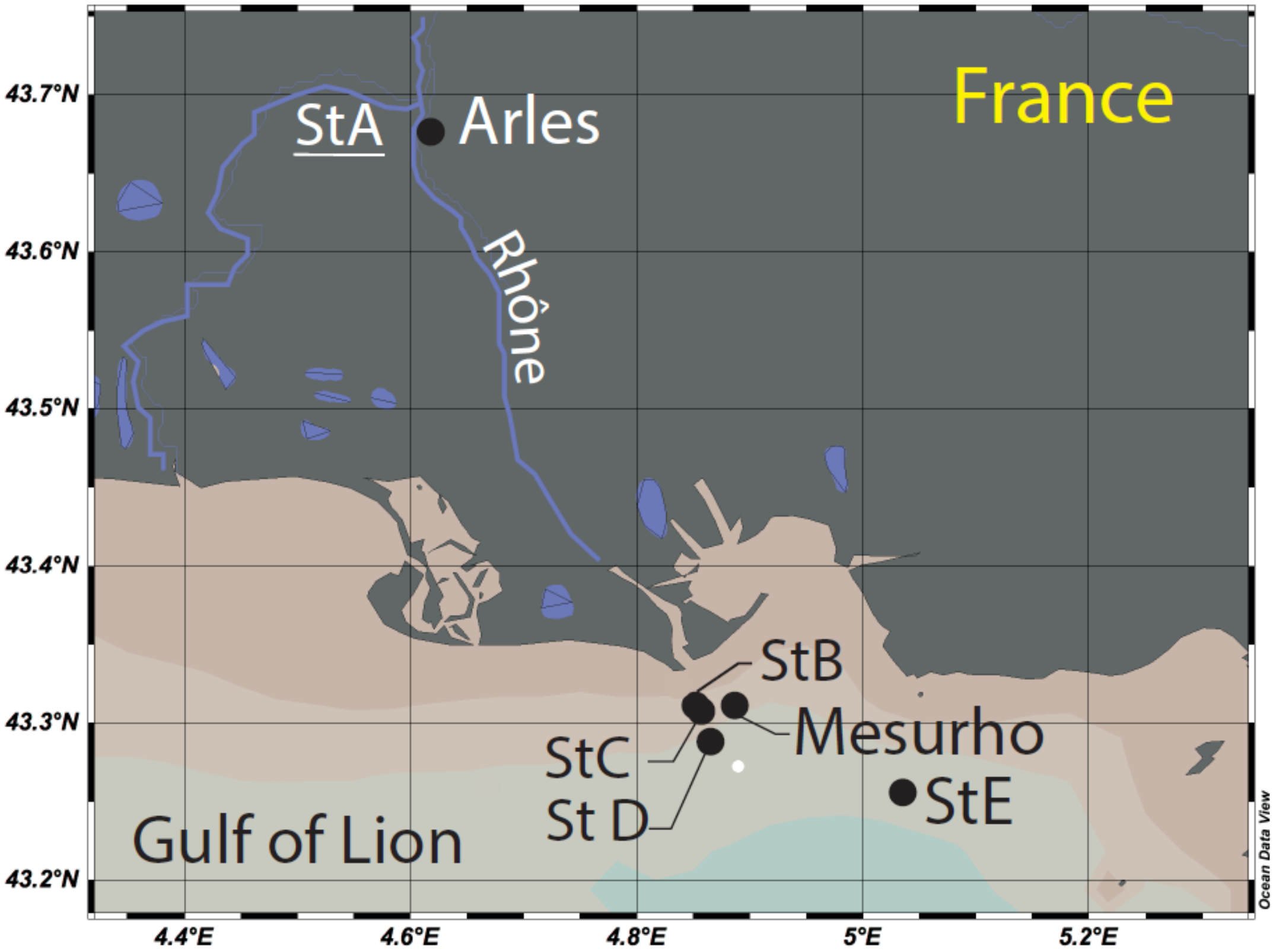

	sampling date	longitude	latitude	salinity
St A	22/02/2012	4.37.16	43. 40.44	0
St B	23/02/2012	4.51.64	43.18.77	15
St C	24/02/2012	4.51.64	43.18.57	33
St D	25/02/2012	4.52.91	43.18.43	39.3
St E	22/02/2012	5.02.57	43.18.89	40
Mesurho		4.51.58	43.19.2	20

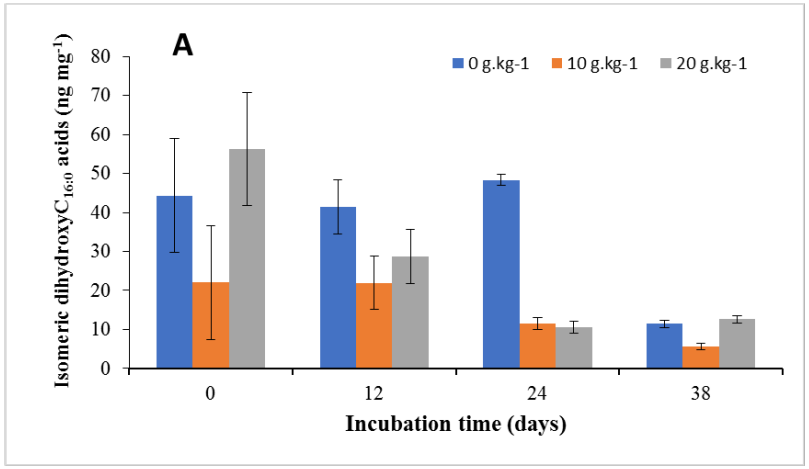
A
0 g.kg-1
10 g.kg-1
20 g.kg-1
Isomeric dihydroxyC16:0 acids (ng mg-1)
0
10
20
30
40
50
60
70
80
0
12
24
38
Incubation time (days)

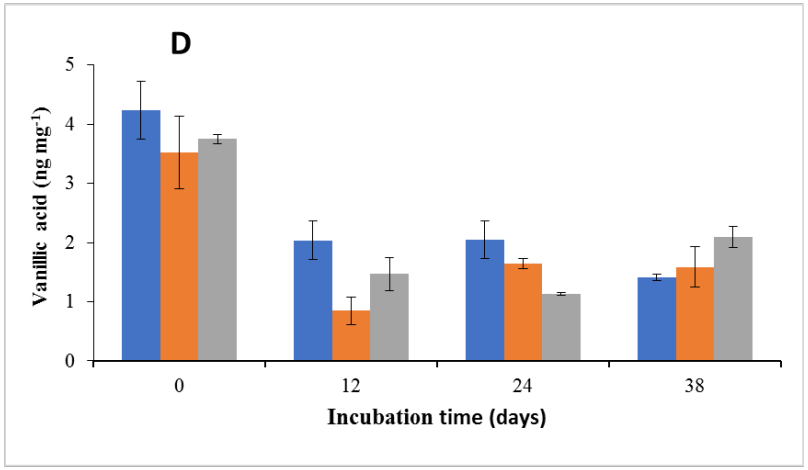
D
Vanillic acid (ng mg-1)
0
1
2
3
4
5
0
12
24
38
Incubation time (days)

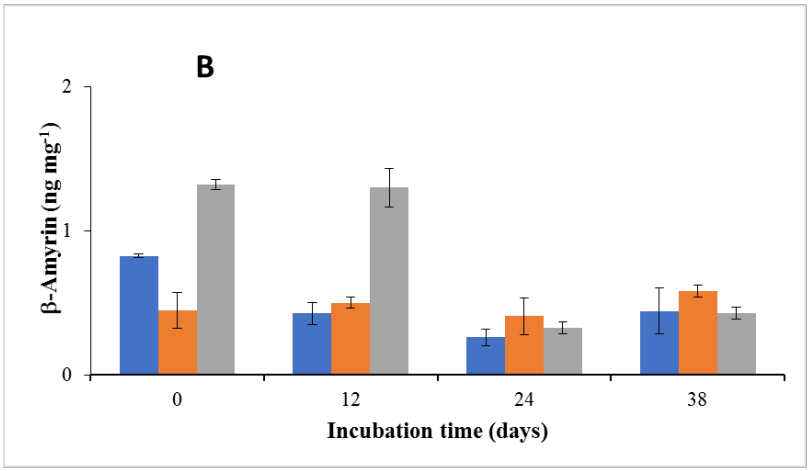
B
β-Amyrin (ng mg-1)
0
1
2
0
12
24
38
Incubation time (days)

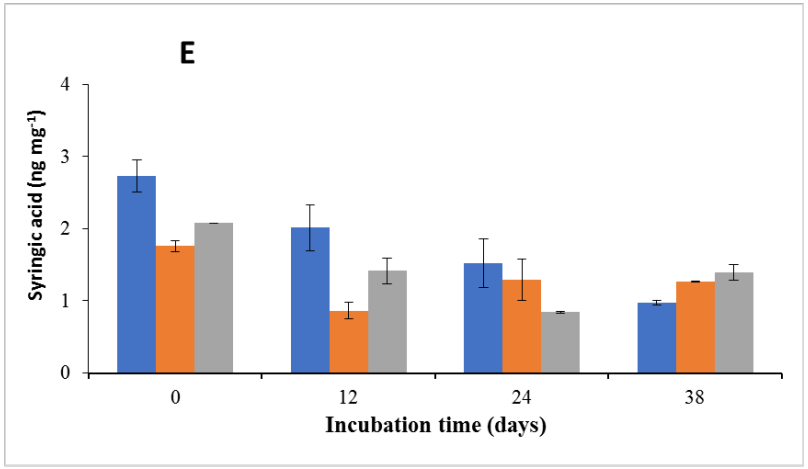
E
Syringic acid (ng mg-1)
0
1
2
3
4
0
12
24
38
Incubation time (days)

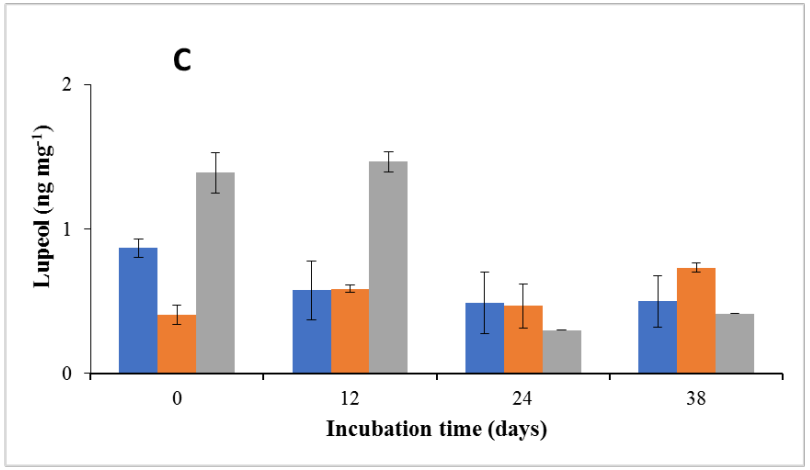
C
Lupeol (ng mg-1)
0
1
2
0
12
24
38
Incubation time (days)

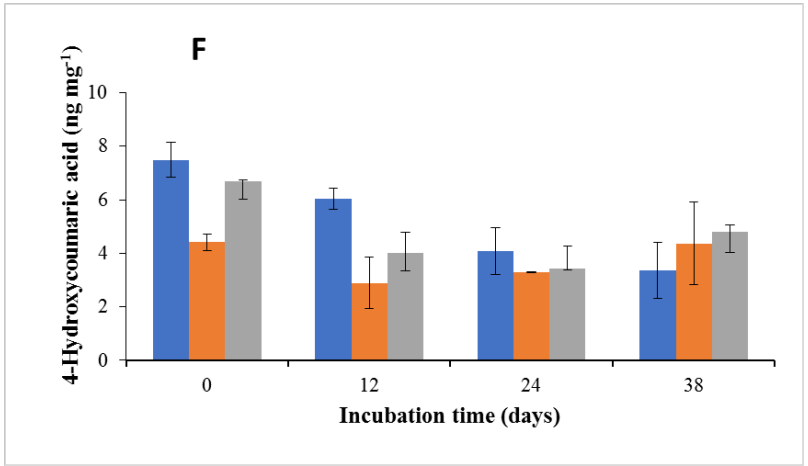
F
4-Hydroxycoumaric acid (ng mg-1)
0
2
4
6
8
10
0
12
24
38
Incubation time (days)

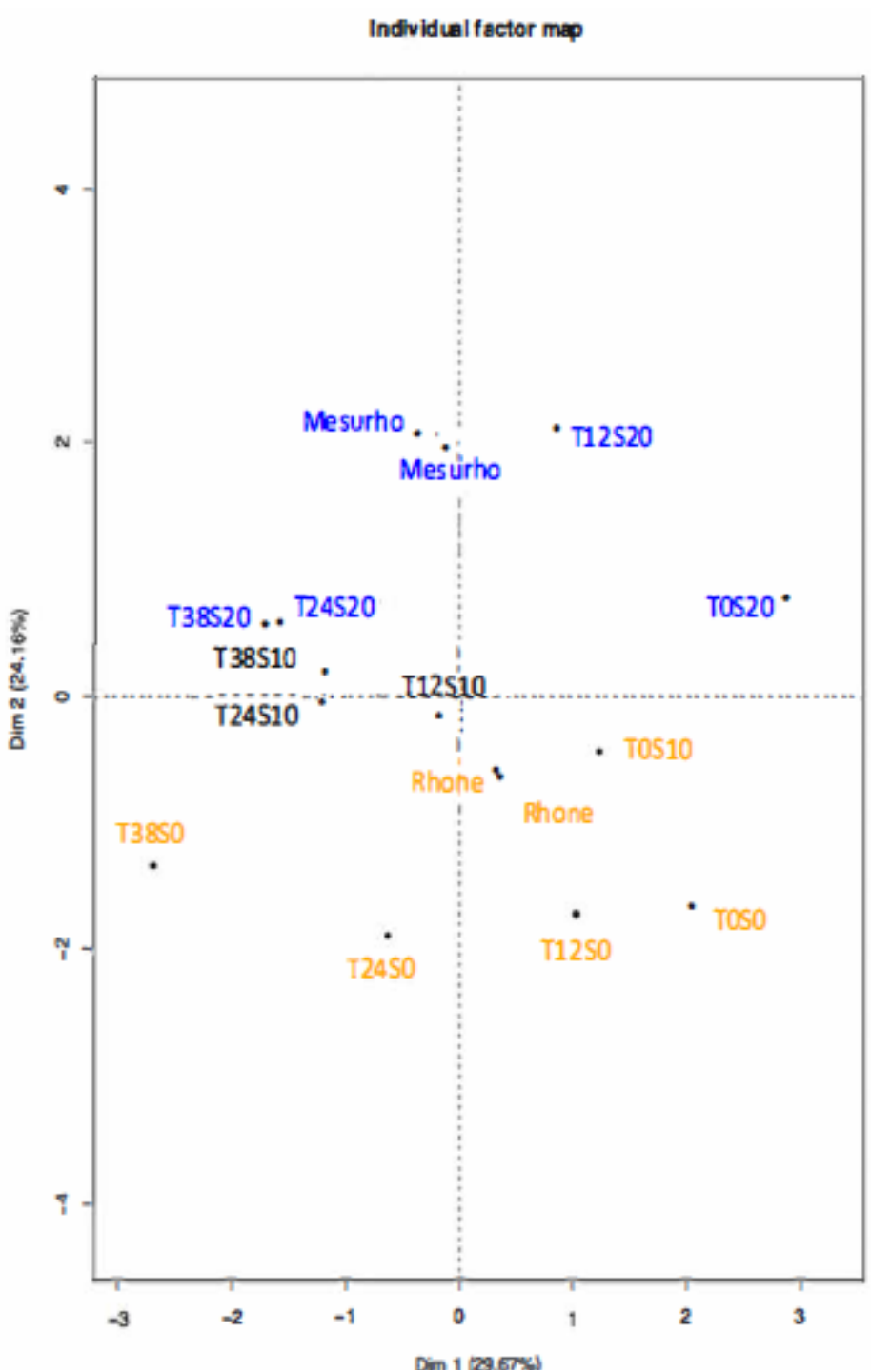
Individual factor map
Mesurho
Mesurho
T12S20
T38S20
T24S20
T0S20
T38S10
T12S10
T24S10
T0S10
Rhone
Rhone
T38S0
T0S0
T12S0
T24S0
Dim 2 (24.16%)
Dim 1 (29.67%)

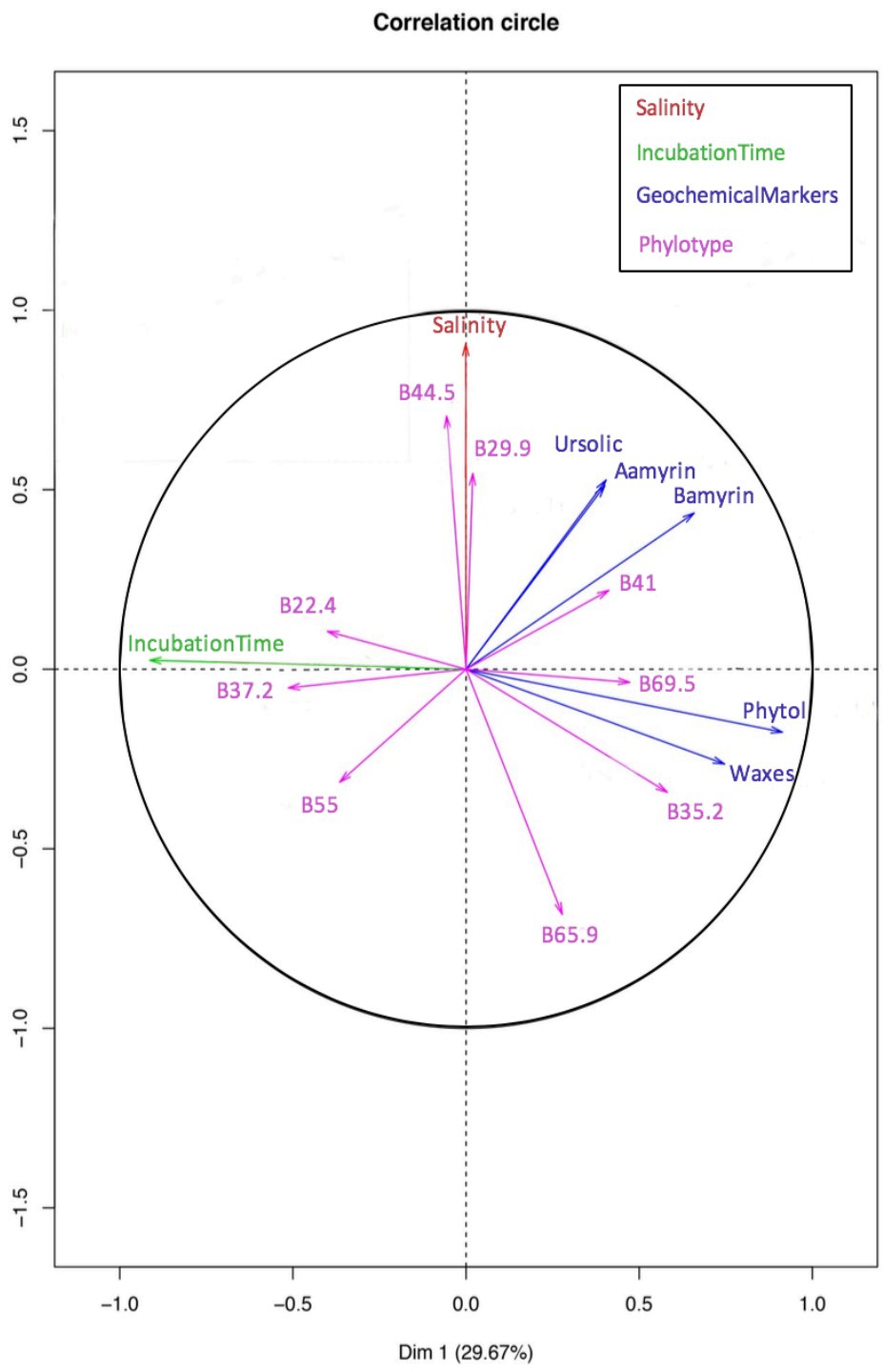
Correlation circle
Salinity
IncubationTime
GeochemicalMarkers
Phylotype
Salinity
B44.5
B29.9
Ursolic
Aamyrin
Bamyrin
B41
B22.4
IncubationTime
B37.2
B69.5
Phytol
Waxes
B55
B35.2
B65.9
Dim 1 (29.67%)

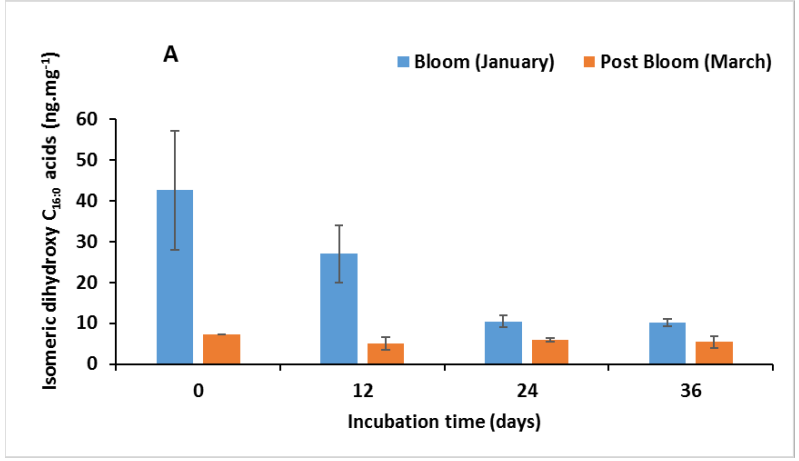
A
Bloom (January)
Post Bloom (March)
Isomeric dihydroxy C16:0 acids (ng.mg-1)
60
50
40
30
20
10
0
0
12
24
36
Incubation time (days)

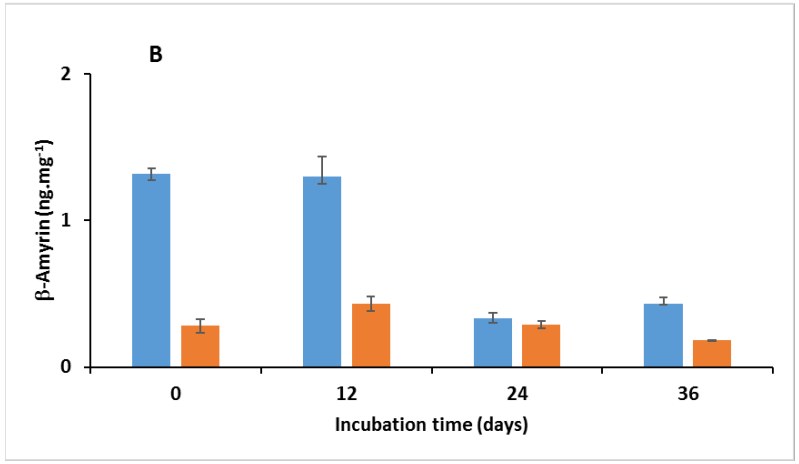
B
β-Amyrin (ng.mg-1)
2
1
0
0
12
24
36
Incubation time (days)

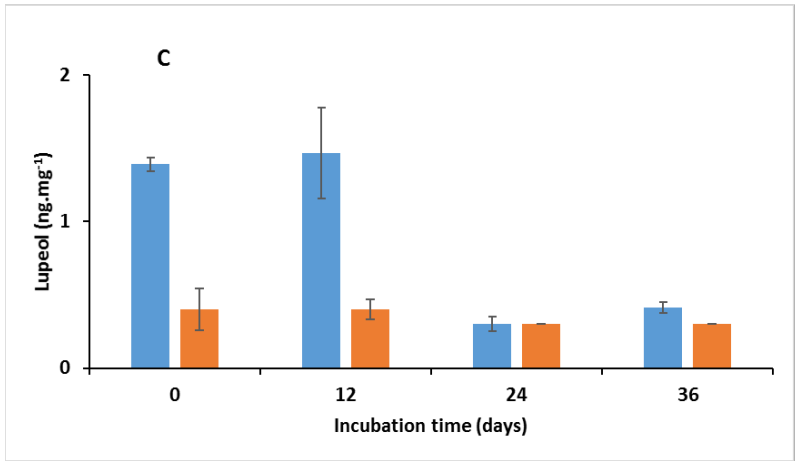
C
Lupeol (ng.mg-1)
2
1
0
0
12
24
36
Incubation time (days)

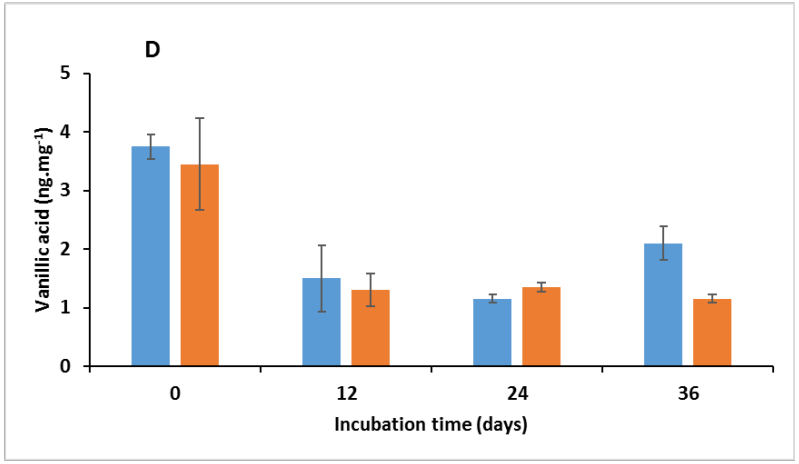
D
Vanillic acid (ng.mg-1)
5
4
3
2
1
0
0
12
24
36
Incubation time (days)

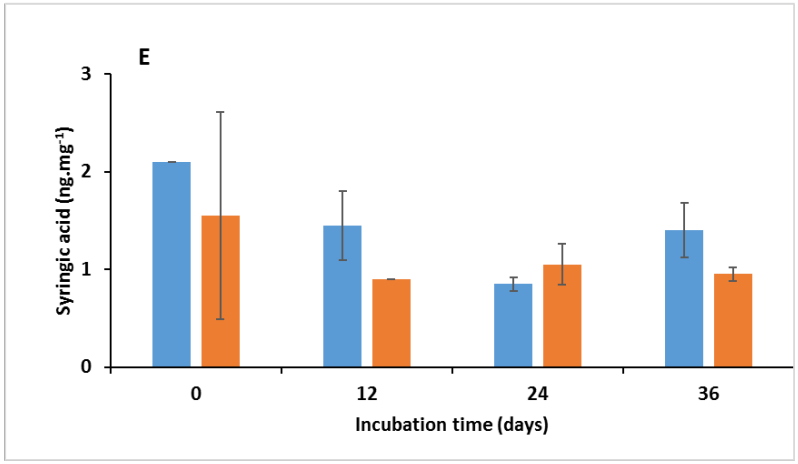
E
Syringic acid (ng.mg-1)
3
2
1
0
0
12
24
36
Incubation time (days)

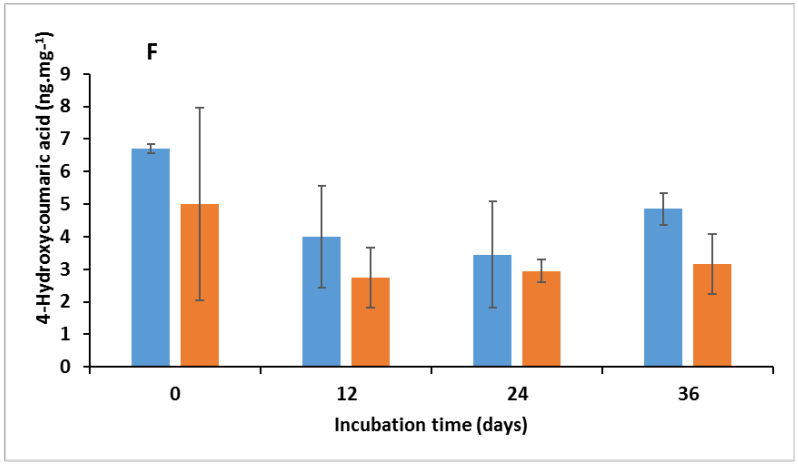
F
4-Hydroxycoumaric acid (ng.mg-1)
9
8
7
6
5
4
3
2
1
0
0
12
24
36
Incubation time (days)

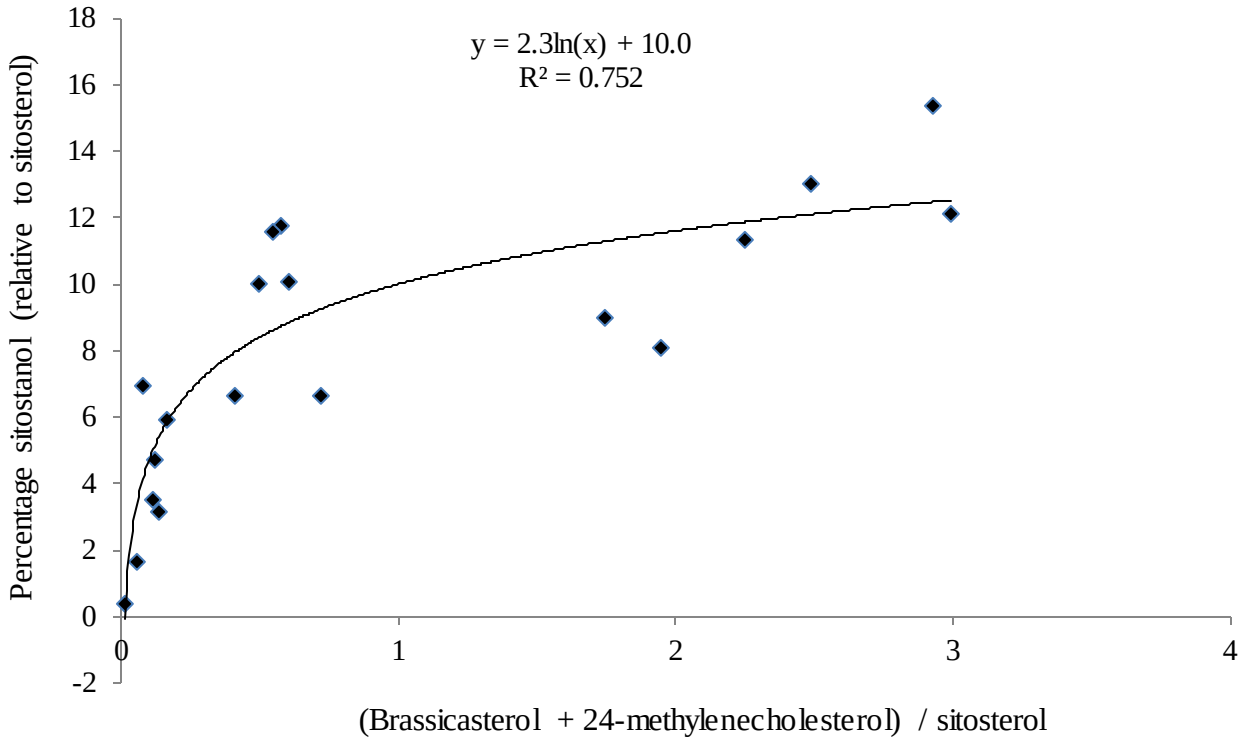
y = 2.3ln(x) + 10.0
R² = 0.752
Percentage sitostanol (relative to sitosterol)
18
16
14
12
10
8
6
4
2
0
-2
0
1
2
3
4
(Brassicasterol + 24-methylenecholesterol) / sitosterol

Order	Family
Actinobacteria	ACK-M1
Alphaproteobacteria	Pelagibacteraceae
	Rhodospirillaceae
	Rhodobacteraceae
Bacteroidia	Porphyromonadaceae
Betaproteobacteria	Comamonadaceae
	Methylophilaceae
	Rhodocyclaceae
Cytophagia	Cytophagaceae
Flavobacteriia	Cryomorphaceae
	Flavobacteriaceae
Gammaproteobacteria	Alteromonadaceae
	Colwelliaceae
	Halomonadaceae
	Oceanospirillaceae
	Pseudoalteromonadaceae
	Sinobacteraceae
Thaumarchaeota	Cenarchaeaceae

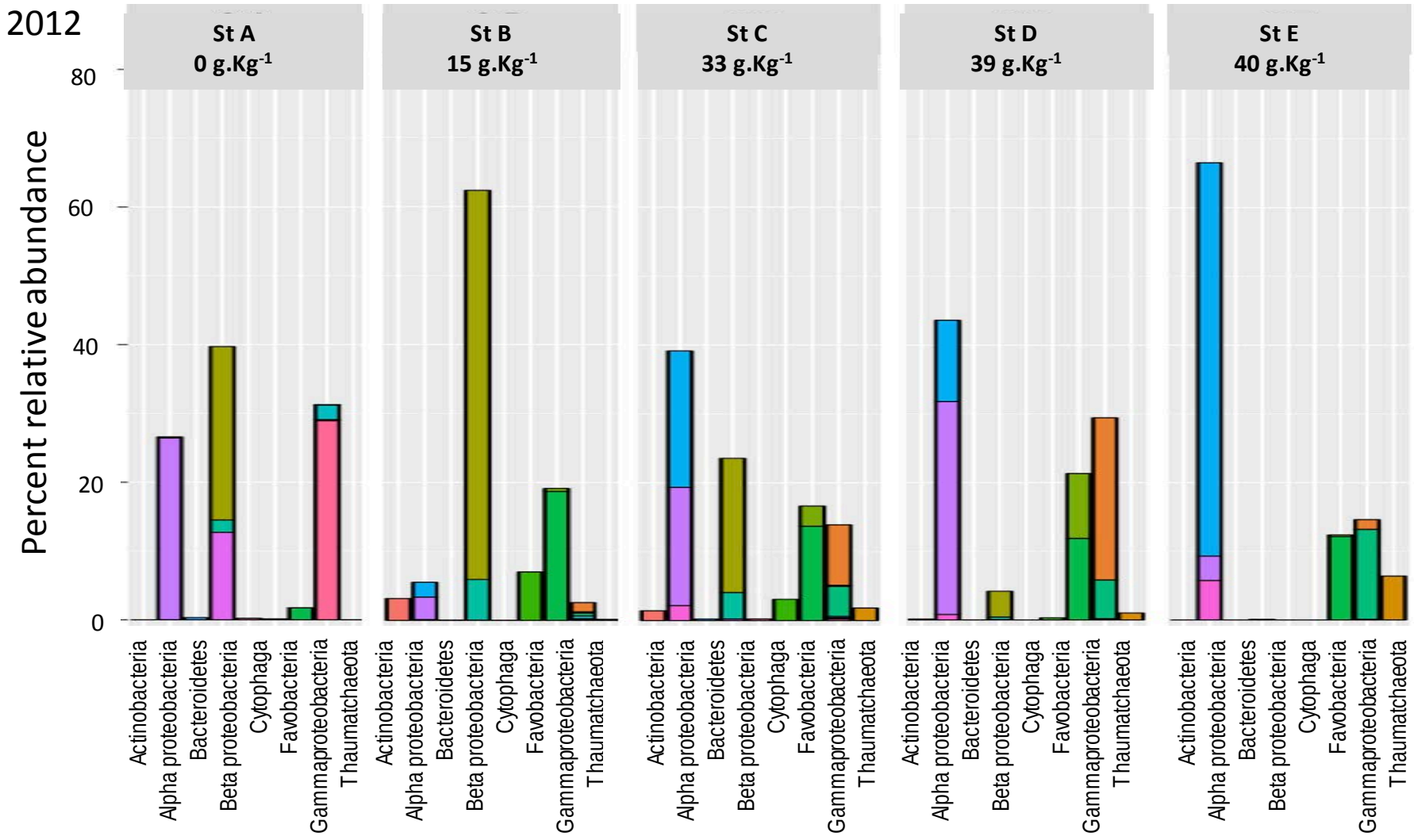

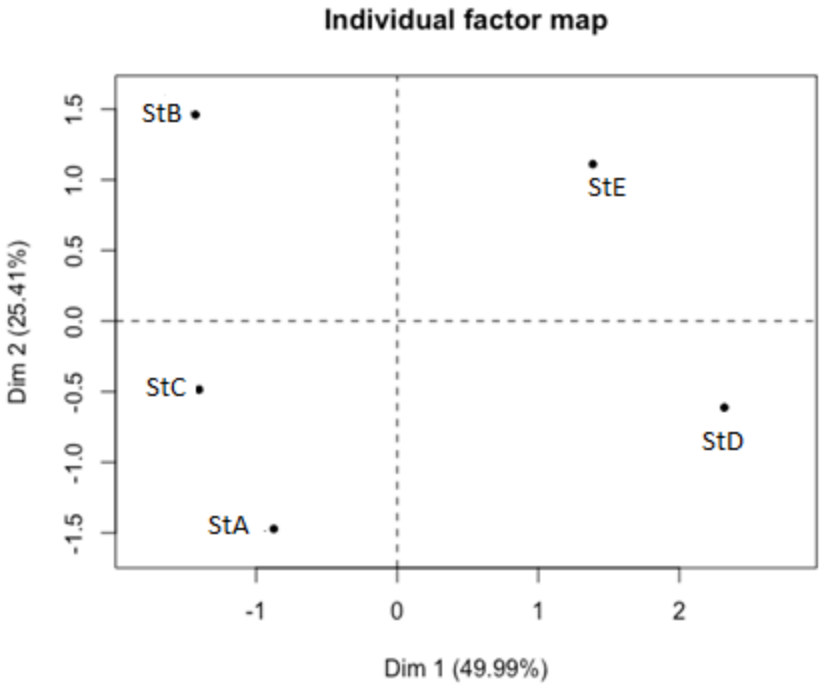
Individual factor map
StB
StE
StC
StD
StA
Dim 2 (25.41%)
Dim 1 (49.99%)
1.5
1.0
0.5
0.0
-0.5
-1.0
-1.5
-1
0
1
2

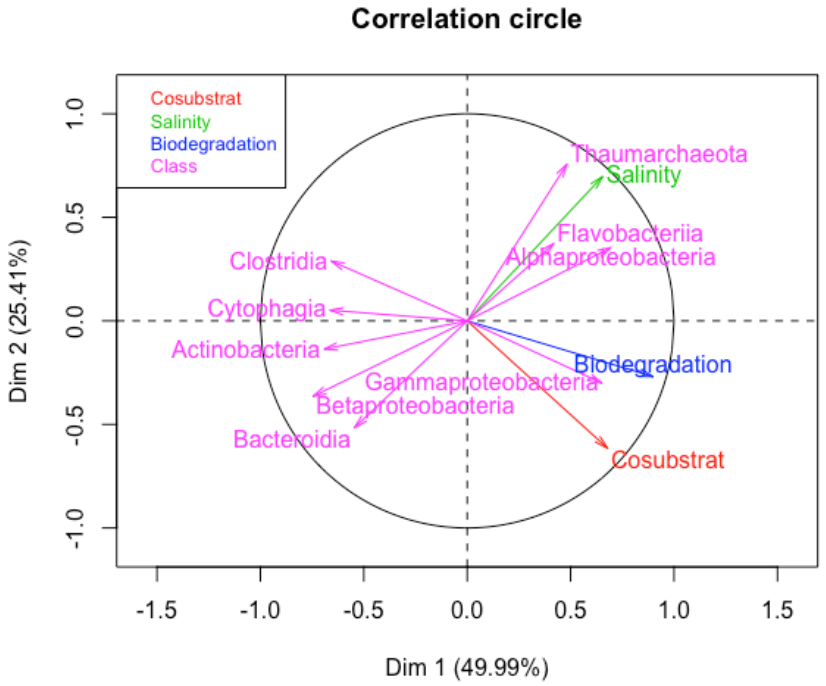
Correlation circle
Cosubstrat
Salinity
Biodegradation
Class
Thaumarchaeota
Salinity
Flavobacteriia
Alphaproteobacteria
Clostridia
Cytophagia
Actinobacteria
Biodegradation
Gammaproteobacteria
Betaproteobacteria
Bacteroidia
Cosubstrat
Dim 2 (25.41%)
Dim 1 (49.99%)
1.0
0.5
0.0
-0.5
-1.0
-1.5
-1.0
-0.5
0.0
0.5
1.0
1.5

Table 1

Origin of the main lipid tracers (See appendix) employed during the present work.

Lipid tracers	Origin	References
9,16- and 10,16-dihydroxyhexadecanoic acids	Cuticular waxes of higher plants	Von Wettstein-Knowles, 1993
α-Amyrin	Angiosperms	Pancost and Boot, 2004; Otto et al., 2005
β-Amyrin	Angiosperms	Pancost and Boot, 2004; Otto et al., 2005
Lupeol	Angiosperms	Pancost and Boot, 2004; Otto et al., 2005
Ursolic acid	Angiosperms	Pancost and Boot, 2004; Otto et al., 2005
Oleanolic acid	Angiosperms	Pancost and Boot, 2004; Otto et al., 2005
Vanillic acid	Vascular plants	Hedges and Mann, 1979
Syringic acid	Angiosperms	Hedges and Mann, 1979
Ferulic acid	Vascular plants (non woody)	Hedges and Mann, 1979
4-Hydroxycoumaric acid	Vascular plants (non woody)	Hedges and Mann, 1979
Brassicasterol	Phytoplankton	Volkman, 2003; Rampen et al., 2010
24-Methylenecholesterol	Diatoms	Volkman, 2003; Rampen et al., 2010
Desmosterol	Diatoms	Volkman, 2003; Rampen et al., 2010
Sitosterol	Phytoplankton and vascular plants	Volkman, 2003
Sitostanol	Biodegradation of sterols	Wakeham, 1989

Table 2 : Phylum-level taxonomic distribution of bacterial and archeal assemblages from sampling stations along salinity gradient at the Rhône river mouth

	salinity	Number of trimmed sequences	Number of observed OTU (97%)	Good's coverage (%)	shannon index	Simpson index
StA	0	74780	52161	85.35	7.75	0.98
StB	15	69753	57801	71.53	5.87	0.93
StC	33	73376	68842	85.70	7.02	0.97
StD	39	55065	42430	72.86	6.39	0.96
StE	40	69146	54486	82.75	6.83	0.97

A

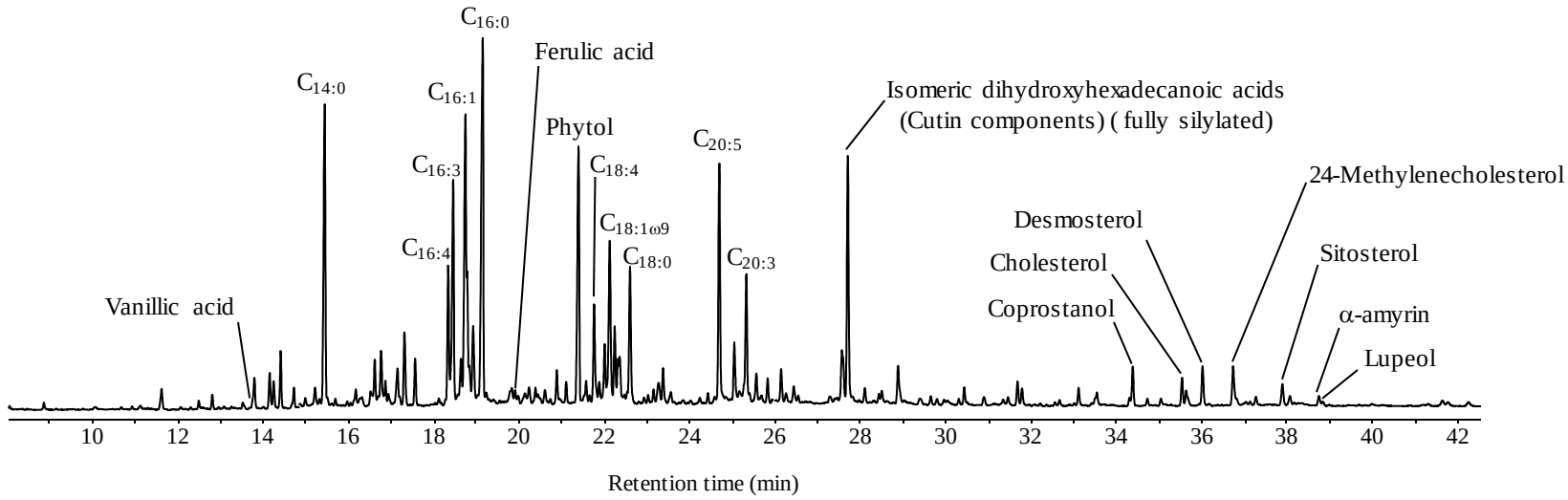
C16:0
Ferulic acid
C14:0
C16:1
Phytol
C16:3
C18:4
C20:5
Isomeric dihydroxyhexadecanoic acids
(Cutin components) (fully silylated)
24-Methylenecholesterol
C18:1ω9
Desmosterol
C16:4
C18:0
C20:3
Sitosterol
Cholesterol
Vanillic acid
Coprostanol
α-amyrin
Lupeol
10 12 14 16 18 20 22 24 26 28 30 32 34 36 38 40 42
Retention time (min)

B

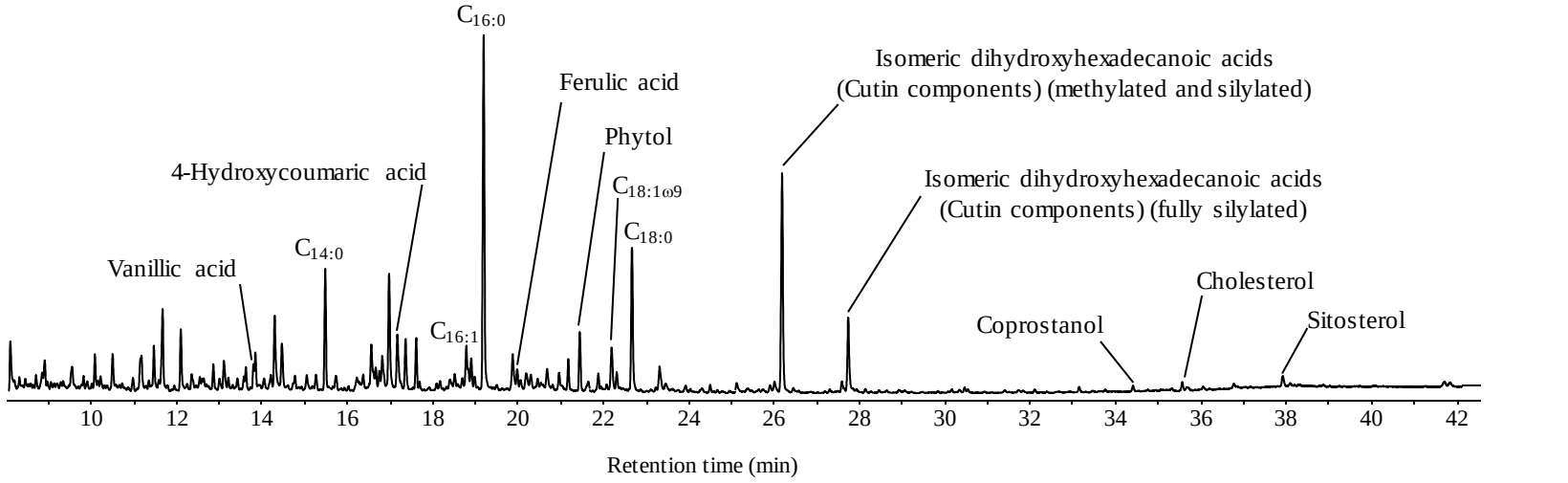
C16:0
Isomeric dihydroxyhexadecanoic acids
(Cutin components) (methylated and silylated)
Ferulic acid
Phytol
4-Hydroxycoumaric acid
C18:1ω9
Isomeric dihydroxyhexadecanoic acids
(Cutin components) (fully silylated)
C18:0
C14:0
Vanillic acid
Cholesterol
C16:1
Coprostanol
Sitosterol
10 12 14 16 18 20 22 24 26 28 30 32 34 36 38 40 42
Retention time (min)

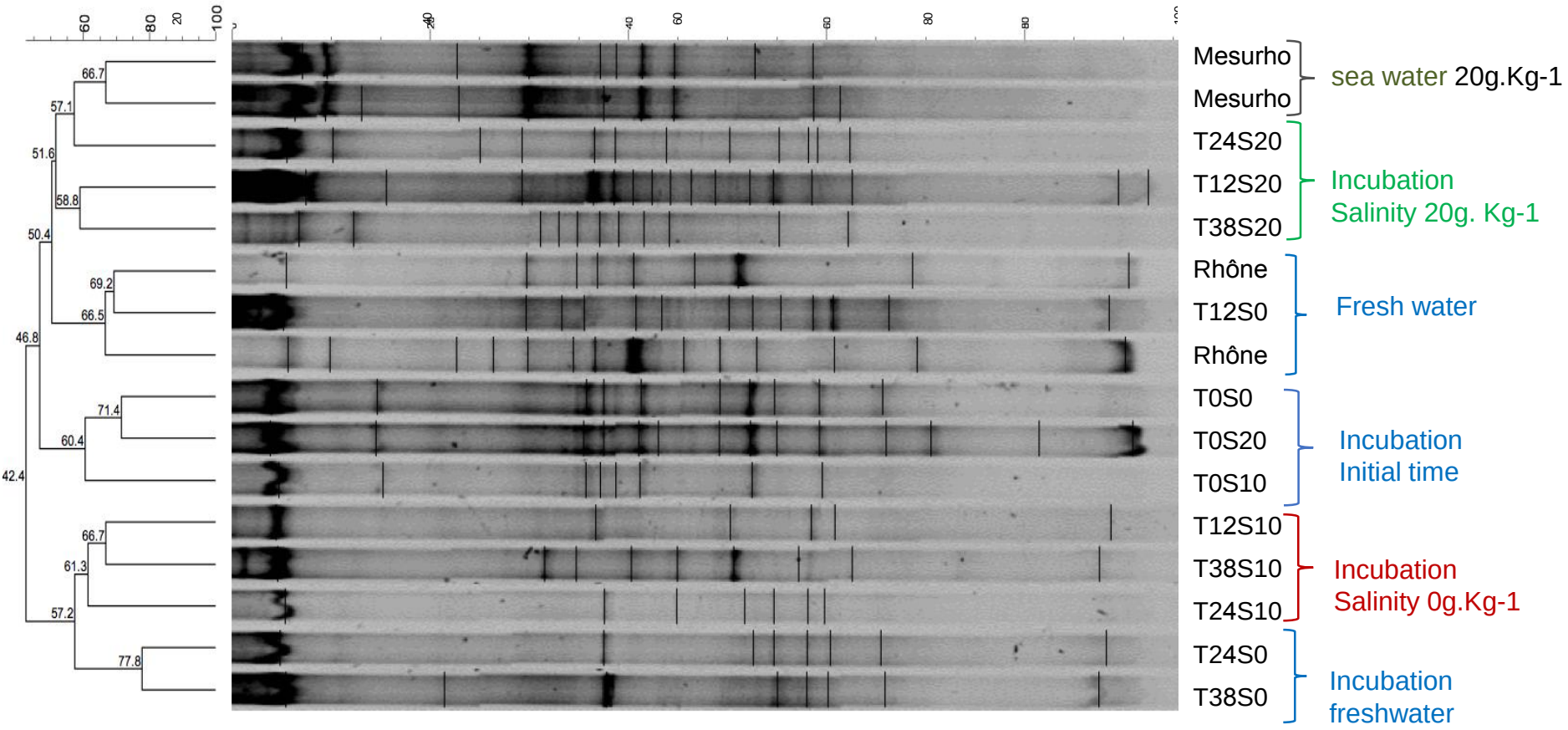
66.7
57.1
51.6
58.8
50.4
69.2
66.5
46.8
71.4
60.4
42.4
66.7
61.3
57.2
77.8
Mesurho
Mesurho
T24S20
T12S20
T38S20
Rhône
T12S0
Rhône
T0S0
T0S20
T0S10
T12S10
T38S10
T24S10
T24S0
T38S0
sea water 20g.Kg-1
Incubation
Salinity 20g. Kg-1
Fresh water
Incubation
Initial time
Incubation
Salinity 0g.Kg-1
Incubation
freshwater

Table S1

Evolution of the concentration (ng mg^{-1}) of vascular plant components during incubations at different salinity conditions

	Sample [a]	α-Amyrin	β-Amyrin	Lupeol	Isomeric dihydroxy $C_{16:0}$ acids[b]
Rhône SPM (Bloom samples)	T0S0	0.7	0.8	0.8	30.1
	T0S0	0.5	0.9	1.0	44.6
	T12S0	0.3	0.5	0.9	24.5
	T12S0	0.2	0.3	0.3	48.5
	T24S0	0.4	0.3	0.8	75.3
	T24S0	0.2	0.2	0.2	11.7
	T38S0	0.2	0.2	0.3	15.8
	T38S0	0.6	0.7	0.8	4.1
	T0S10	0.5	0.6	0.5	24.6
	T0S10	0.2	0.3	0.3	15.5
	T12S10	0.5	0.5	0.6	30.3
	T12S10	0.5	0.6	0.6	10.5
	T24S10	0.2	0.2	0.3	5.2
	T24S10	0.5	0.6	0.7	16.1
	T38S10	0.4	0.6	0.8	4.0
	T38S10	0.4	0.5	0.7	4.9
	T0S20	1.1	1.4	1.3	22.0
	T0S20	1.1	1.3	1.5	63.2
	T12S20	1.0	1.1	1.0	36.8
	T12S20	3.7	1.5	1.9	17.2
	T24S20	0.4	0.4	0.4	8.3
	T24S20	0.2	0.3	0.2	12.6
	T38S20	0.3	0.4	0.4	8.9
	T38S20	0.3	0.5	0.5	11.4
Rhône SPM (Post-bloom samples)	T0S20	0.1	0.2	0.2	7.3
	T0S20	0.3	0.3	0.6	7.3
	T12S20	0.2	0.4	0.3	8.6
	T12S20	0.3	0.5	0.5	1.5
	T24S20	0.2	0.3	0.3	6.4
	T24S20	0.2	0.3	0.3	5.4
	T38S20	0.1	0.2	0.3	4.7
	T38S20	0.1	0.2	0.3	6.2

[a] T = incubation time (0 ; 12 ; 24 or 38 days), S = Salinity (0 ; 10 or 20 g kg^{-1})

[b] Cuticular wax components

Table S2

Evolution of the concentration (ng mg^{-1}) of phenolic acids during the different incubations

	Sample [a]	Vanillic acid	Syringic acid	4-Hydroxycoumaric acid
Rhône SPM (Bloom samples)	T0S0	3.5	2.4	6.6
	T0S0	4.9	3.1	8.4
	T12S0	2.5	2.5	6.6
	T12S0	1.6	1.6	5.5
	T24S0	2.5	2.0	5.3
	T24S0	1.6	1.0	2.9
	T38S0	1.5	1.0	4.8
	T38S0	1.3	0.9	1.9
	T0S10	4.4	1.9	4.8
	T0S10	2.7	1.7	4.0
	T12S10	1.2	1.0	4.2
	T12S10	0.5	0.7	1.6
	T24S10	1.5	0.9	3.3
	T24S10	1.8	1.7	3.3
	T38S10	1.1	1.3	2.2
	T38S10	2.1	1.2	6.6
	T0S20	3.9	2.1	6.6
	T0S20	3.6	2.1	6.8
	T12S20	1.9	1.7	5.1
	T12S20	1.1	1.2	2.9
	T24S20	1.1	0.9	2.3
	T24S20	1.2	0.8	4.6
	T38S20	1.9	1.2	4.5
	T38S20	2.3	1.6	5.2
Rhône SPM (Post-bloom samples)	T0S20	2.9	0.8	2.9
	T0S20	4.0	2.3	7.1
	T12S20	1.5	0.9	3.4
	T12S20	1.1	0.9	2.1
	T24S20	1.4	1.2	3.2
	T24S20	1.3	0.9	2.7
	T38S20	1.2	1.0	3.8
	T38S20	1.1	0.9	2.5

[a] T = incubation time (0, 12, 24 or 38 day), S = Salinity (0 , 10 or 20 g kg^{-1})

Table S3 :

(Brassicasterol + 24-methylenecholesterol) / sitosterol	Sitostanol (%)
0.012	0.432
0.054	1.697
0.167	5.978
0.121	4.734
0.114	3.573
0.411	6.656
0.135	3.183
0.722	6.652
0.492	10.025
0.078	6.951
0.601	10.128
0.579	11.803
0.548	11.619
1.947	8.133
2.486	13.043
2.994	12.149
1.746	9.017
2.926	15.393
2.250	11.376

Table S4

Phylum	StA	StB	StC	StD	StrE
Other	0.082	0.085	1.343	0.930	0.467
Crenarchaeota	0.045	0.209	1.519	0.992	3.838
Euryarchaeota	0.004	0.068	1.184	0.577	3.467
[Parvarchaeota]	0.000	0.000	0.000	0.000	0.000
Acidobacteria	3.272	0.029	0.144	0.011	0.000
Actinobacteria	3.920	10.050	6.766	3.182	5.261
Armatimonadetes	0.074	0.000	0.000	0.000	0.000
BRC1	0.078	0.000	0.000	0.000	0.000
Bacteroidetes	6.664	24.997	20.023	23.266	15.031
Chlamydiae	0.000	0.005	0.000	0.000	0.000
Chlorobi	0.349	0.017	0.000	0.003	0.000
Chloroflexi	0.472	0.201	0.539	0.304	1.004
Cyanobacteria	0.000	0.000	0.000	0.000	0.000
Elusimicrobia	0.008	0.000	0.000	0.000	0.000
FCPU426	0.000	0.000	0.000	0.000	0.000
Fibrobacteres	0.000	0.000	0.079	0.000	0.000
Firmicutes	2.122	0.121	1.364	0.057	0.146
Fusobacteria	0.161	0.024	0.053	0.022	0.000
GN04	0.000	0.000	0.000	0.000	0.000
Gemmatimonadetes	0.377	0.041	0.238	0.121	0.326
Lentisphaerae	0.000	0.000	0.036	0.005	0.020
NC10	0.008	0.000	0.000	0.000	0.000
Nitrospirae	0.511	0.012	0.098	0.000	0.000
OP3	0.000	0.000	0.000	0.000	0.000
PAUC34f	0.000	0.000	0.089	0.019	0.080
Planctomycetes	0.348	0.073	0.136	0.084	0.600
Proteobacteria	77.619	63.525	63.894	69.312	65.715
SAR406	0.000	0.085	0.851	0.571	1.915
SBR1093	0.004	0.058	0.717	0.396	1.401
Spirochaetes	0.012	0.000	0.070	0.000	0.000
TM6	0.000	0.000	0.000	0.000	0.000
TM7	0.072	0.000	0.000	0.000	0.000
Tenericutes	0.006	0.000	0.000	0.000	0.000
Verrucomicrobia	3.668	0.398	0.660	0.143	0.718
WS3	0.128	0.002	0.079	0.003	0.000
ZB3	0.000	0.000	0.119	0.005	0.010

Table S5 :

Phylum	Class	Order	Family	StA	StB	StC	StD	StE
Actinobacteria	Actinobacteria	Actinomycetales	ACK-M1	0,000	3,309	1,484	0,136	0,000
Bacteroidetes	Bacteroidia	Bacteroidales	Porphyromonadaceae	0,359	0,048	0,231	0,005	0,000
Bacteroidetes	Cytophagia	Cytophagales	Cytophagaceae	0,148	7,343	3,217	0,313	0,000
Bacteroidetes	Flavobacteriia	Flavobacteriales	Cryomorphaceae	0,000	0,445	3,052	9,539	0,255
Bacteroidetes	Flavobacteriia	Flavobacteriales	Flavobacteriaceae	1,751	15,935	12,657	11,783	12,877
Crenarchaeota	Thaumarchaeota	Cenarchaeales	Cenarchaeaceae	0,011	0,153	1,903	1,028	6,780
Proteobacteria	Alphaproteobacteria	Rickettsiales	Pelagibacteraceae	0,179	2,240	20,627	11,960	60,728
Proteobacteria	Alphaproteobacteria	Rhodobacterales	Rhodobacteraceae	29,662	3,405	17,895	31,328	3,772
Proteobacteria	Betaproteobacteria	Burkholderiales	Comamonadaceae	16,487	58,260	20,236	3,734	0,082
Proteobacteria	Betaproteobacteria	Methylophilales	Methylophilaceae	2,015	6,142	3,999	0,369	0,016
Proteobacteria	Betaproteobacteria	Methylophilales	Methylophilaceae	2,384	0,423	0,212	0,033	0,049
Proteobacteria	Betaproteobacteria	Rhodocyclales	Rhodocyclaceae	14,283	0,044	0,240	0,056	0,000
Proteobacteria	Gammaproteobacteria	Alteromonadales	Alteromonadaceae	0,000	1,393	9,153	23,855	1,496
Proteobacteria	Gammaproteobacteria	Alteromonadales	Colwelliaceae	0,021	0,170	0,113	0,023	0,000
Proteobacteria	Gammaproteobacteria	Oceanospirillales	Halomonadaceae	0,021	0,432	4,546	5,674	13,888
Proteobacteria	Gammaproteobacteria	Oceanospirillales	Oceanospirillaceae	0,000	0,052	0,000	0,000	0,000
Proteobacteria	Gammaproteobacteria	Vibrionales	Pseudoalteromonadaceae	0,169	0,065	0,188	0,070	0,058
Proteobacteria	Gammaproteobacteria	Xanthomonadales	Sinobacteraceae	32,511	0,140	0,245	0,093	0,000